PHYSICAL REVIEW D **90,** 094508 (2014)

Phase diagram of nondegenerate twisted mass fermions

Derek P. Horkel[*] and Stephen R. Sharpe[†]

Physics Department, University of Washington, Seattle, Washington 98195-1560, USA

(Received 18 September 2014; published 24 November 2014)

We determine the phase diagram and pion spectrum for Wilson and twisted-mass fermions in the presence of nondegeneracy between the up and down quarks *and* discretization errors, using Wilson and twisted-mass chiral perturbation theory. We find that the *CP*-violating phase of the continuum theory (which occurs for sufficiently large nondegeneracy) is continuously connected to the Aoki phase of the lattice theory with degenerate quarks. We show that discretization effects can, in some cases, push simulations with physical masses closer to either the *CP*-violating phase or another phase not present in the continuum, so that at sufficiently large lattice spacings physical-point simulations could lie in one of these phases.

DOI: 10.1103/PhysRevD.90.094508 PACS numbers: 12.38.Gc, 11.30.Rd, 12.38.-t, 12.39.Fe

I. INTRODUCTION

It has long been known, in the case of three nondegenerate light quarks, that there is a transition to a *CP*-violating phase when one of the quark masses becomes sufficiently negative [1]. For example, using leading-order (LO) SU(3) chiral perturbation theory (χPT), and fixing m_d and m_s, the transition occurs when $m_u = -m_d m_s/(m_d + m_s)$ [2]. The neutral pion becomes massless on the transition line, and within the new phase the chiral order parameter, $\langle\Sigma\rangle$, becomes complex. For physical QCD this is mostly a curiosity, since increasingly accurate determinations of the quark masses indicate clearly that all are positive relative to one another [3,4]. Thus physical QCD, despite the nondegeneracy of the up and down quarks, lies away from the critical line.

For lattice QCD (LQCD), however, the situation is less clear. The position of the transition can be shifted closer to the physical point by discretization effects. Indeed, it is well known that, with degenerate Wilson-like[1] fermions, discretization effects can lead to the appearance of a new phase —the Aoki phase—in which isospin is spontaneously broken and $\langle\Sigma\rangle$ is complex [5,6]. In addition, advances in simulations now allow calculations to be done at the physical light-quark masses, including, very recently, the physical nondegeneracy between up and down quarks [7]. It is thus natural to ask how, in LQCD with nondegenerate quarks, discretization effects change the position and nature of the *CP*-violating phase. This question is particularly acute in the case of twisted-mass fermions, where additional symmetry breaking is explicitly included.

In this paper we address this question for Wilson-like and twisted-mass lattice fermions. We do so using χPT, specifically the versions of χPT in which the effects of discretization have been included. Our work also allows us to address a related issue: in what way is the *CP*-violating phase of the continuum theory related to the Aoki phase of the lattice theory?[2]

Since twisted-mass QCD is only defined for even numbers of fermion flavors [9], a necessary step for our work is to rephrase the continuum SU(3) χPT analysis of Ref. [2] in the two-flavor theory obtained by integrating out the strange quark. This requires that the contributions of one of the next-to-leading-order (NLO) low-energy coefficients (ℓ_7) be treated as parametrically larger than the others. Thus we are led to a somewhat nonstandard power counting, but one which reproduces the SU(3) phase diagram, including the *CP*-violating phase, within SU(2) χPT. This approach has been used before along the line $m_u = -m_d$ [10]; here we extend the analysis to arbitrary mass splitting. Similar work has also been done recently in the context of an effective theory including the η meson [11].

The organization of this article is as follows. In Sec. II we briefly recall the results for the phase structure and pion masses at LO in SU(2) and SU(3) χPT, and show how they differ. Section III describes the matching of SU(2) and SU(3) χPT. In Sec. IV, we recall briefly how discretization effects are incorporated in χPT for degenerate Wilson-like fermions, and the resulting phase structure. We then present our first new results: the phase diagram including both discretization effects and nondegeneracy. In Sec. V we move onto twisted-mass fermions, focusing first on the phase diagram and pion masses in the case of maximal twist, where most simulations have been done because of the property of automatic $\mathcal{O}(a)$ improvement [9]. It is nevertheless interesting to understand how the results with

[*]dhorkel@uw.edu
[†]srsharpe@uw.edu

[1]"Wilson-like" indicates that the analysis holds for both Wilson fermions and various improvements thereof, in particular for nonperturbatively $\mathcal{O}(a)$-improved Wilson fermions.

[2]This issue has been raised previously by Mike Creutz and his conjectured answer is confirmed by the present analysis [8].

untwisted and maximally twisted fermions are connected, and so, in Sec. VI, we discuss the phase diagram for general twist.

Up to this stage, our analysis is done using the LO terms due to the average quark mass, discretization effects and nondegenerate quark masses. To understand how robust the results are we consider, in Sec. VII, the impact of including the next higher-order terms in our power counting. Some conclusions are collected in Sec. VIII.

II. CONTINUUM VACUUM STRUCTURE AT LEADING ORDER IN χPT

In this section we review the vacuum structure predicted by LO χPT for both two and three light flavors. The LO chiral Lagrangian in Euclidean space-time is, for any number of light flavors,

$$\mathcal{L}_\chi = \frac{f^2}{4}\mathrm{tr}[\partial_\mu \Sigma \partial_\mu \Sigma^\dagger - (\chi\Sigma^\dagger + \Sigma\chi^\dagger)], \tag{1}$$

where $\Sigma \in \mathrm{SU}(N_f)$ and $\chi = 2B_0 M$ (with M the mass matrix), while $f \sim 92$ MeV and B_0 are low-energy constants (LECs).

For two light flavors the chiral order parameter can be parametrized as $\langle\Sigma\rangle = \exp(i\theta\hat{n}\cdot\vec{\tau})$. Although the mass matrix $M = \mathrm{diag}(m_u, m_d)$ has both singlet and triplet components, the leading-order potential depends only on the former

$$\mathcal{V}_{\mathrm{SU}(2),\mathrm{LO}} = -\frac{f^2}{4}\mathrm{tr}[\chi\Sigma^\dagger + \Sigma\chi^\dagger] = -\frac{f^2}{2}\cos\theta\,\mathrm{tr}[\chi] = -f^2\cos\theta\,\chi_\ell. \tag{2}$$

In the last step we have defined the convenient quantity $\chi_\ell = B_0(m_u + m_d)$. The potential is minimized at $\theta = 0$ if $\chi_\ell > 0$ and at $\theta = \pi$ if $\chi_\ell < 0$, resulting in the phase diagram sketched in Fig. 1. In terms of the behavior of the condensate, this is a first-order phase transition at which the condensate flips sign. This characterization is somewhat misleading, however, because the two sides of the transition are related by a nonanomalous flavor rotation. Such a transformation can change $M \to -M$ and $\Sigma \to -\Sigma$, while leaving physics unchanged. Thus by adding an extra dimension to the phase diagram (as we will do later) one finds that the two sides are connected.

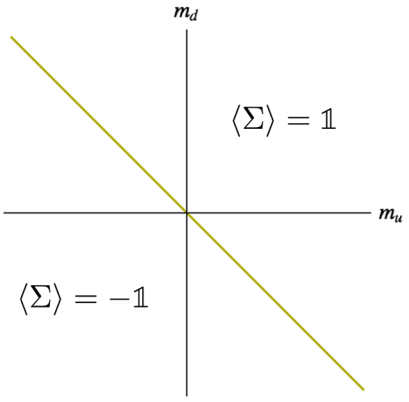

FIG. 1 (color online). Phase diagram at lowest order in SU(2) χPT.

Expanding the potential about its minimum using $\Sigma = \langle\Sigma\rangle \exp(i\vec{\pi}\cdot\vec{\tau}/f)$, we find the standard LO result for the pion masses, $m_\pi^2 = |\chi_\ell|$. These thus vanish along the phase transition line. That they vanish at the origin follows from Goldstone's theorem due to the spontaneous breaking of the exact axial symmetry. That they vanish away from the origin along the transition line is not expected from symmetry arguments, and indeed holds, as we will see, only at LO in χPT.

The phase diagram of the three-flavor theory has a more interesting structure, as elucidated most extensively by Creutz [2]. Since $m_s \gg m_u, m_d$ in nature, it is natural to hold m_s fixed and vary the other two quark masses. The resulting phase diagram at LO is sketched in Fig. 2. The "normal" region, in which $\langle\Sigma\rangle = \mathbb{1}$, ends at a transition line along which m_{π^0} vanishes. This occurs (for fixed $m_s > 0$) when one of the other masses, say m_u, becomes sufficiently negative. The explicit expression for the neutral pion mass in this phase is

$$m^2_{\pi^0\mathrm{SU}(3)} = \frac{2}{3}B_0\left(m_u + m_d + m_s - \sqrt{m_u^2 + m_d^2 + m_s^2 - m_u m_d - m_u m_s - m_d m_s}\right), \tag{3}$$

which vanishes when $m_u = -m_d m_s/(m_d + m_s)$. The charged pions remain massive throughout the normal phase except at the origin.

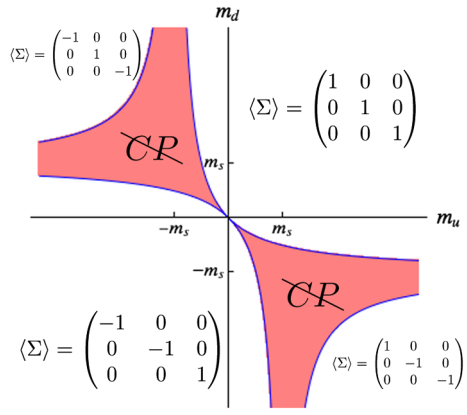

FIG. 2 (color online). Phase diagram at lowest order in SU(3) χPT with fixed strange-quark mass. Equations for the positions of phase transition lines are given in the text.

Moving outside the normal phase one enters a CP-violating phase in which the condensate is complex. The explicit form is

$$\langle\Sigma\rangle = \begin{pmatrix} \exp i\phi & 0 & 0 \\ 0 & \exp i\psi & 0 \\ 0 & 0 & \exp -i(\phi+\psi) \end{pmatrix} \tag{4}$$

where the phases satisfy

$$m_u \sin\phi = m_d \sin\psi = -m_s \sin(\phi+\psi). \tag{5}$$

In this case there is a genuine phase transition at the boundary. It is of second order: $\langle\Sigma\rangle$ is continuous, and a single pion becomes massless.

The phase diagram is symmetric under both $m_u \leftrightarrow m_d$ interchange and inversion through the origin (with m_s fixed). Inversion is brought about by a nonanomalous axial isospin transformation, which also changes the condensate as shown in Fig. 2. We note that the CP-violating region is of finite width.[3] Specifically, as one moves away from the origin along the $m_u = -m_d$ diagonal, the width of this region grows proportionally to $(m_u - m_d)^2/m_s$.

As the figure shows, there are additional phase boundaries in the second and fourth quadrants. These occur, however, when $|m_u|, |m_d| > |m_s|$, and thus lie far from the region of physical interest. In the rest of our analysis, we consider only the region in which $|m_u|, |m_d| \ll |m_s|$, and thus zoom in on the vicinity of the origin in Fig. 2.

III. MATCHING SU(2) AND SU(3) χPT FOR NONDEGENERATE QUARKS

If we choose the quark masses to satisfy $|m_u|, |m_d| \ll |m_s| \ll \Lambda_{\rm QCD}$, then the properties of pions can be simultaneously described by both SU(2) and SU(3) χPT, and the predictions of the two theories must agree. The results of the previous section show that this is not the case if we work to LO in both theories—the CP-violating phase is absent in SU(2) χPT. The discrepancy is resolved by noting that the CP-violating phase has a width proportional to $(m_u - m_d)^2$, indicating that it arises at NLO in SU(2) χPT. In this section we recall how the two theories are matched, and show how the CP-violating phase can then be obtained in SU(2) χPT when including the resulting NLO term.

To do the matching, one considers quantities accessible in both SU(2) and SU(3) theories, namely pion masses and scattering amplitudes. Expanding the LO SU(3) result in powers of $m_{u,d}/m_s$, the leading terms match with the LO SU(2) result, while the first subleading terms match with an NLO SU(2) contribution. The subleading terms in the SU(3) results are in fact proportional to $(m_u - m_d)^2$, because they arise from intermediate η propagators and involve two factors of the $\pi^0 - \eta$ mixing amplitude. The only source of such mass dependence at NLO in the SU(2) theory is the ℓ_7 term in the NLO potential

$$\mathcal{V}_{\rm SU(2)\,NLO} = -\frac{\ell_3}{16}[{\rm tr}(\chi^\dagger\Sigma + \Sigma^\dagger\chi)]^2 + \frac{\ell_7}{16}[{\rm tr}(\chi^\dagger\Sigma - \Sigma^\dagger\chi)]^2. \tag{6}$$

Writing χ as

$$\chi = \chi_\ell \mathbb{1} + \epsilon\tau_3, \quad \text{with} \quad \epsilon = B_0(m_u - m_d), \tag{7}$$

we see that only the ϵ part contributes to the ℓ_7 term. Thus this term leads to contributions proportional to $(m_u - m_d)^2$. Other NLO contributions (i.e. those proportional to different NLO LECs or coming from loops) do not have this mass dependence.

The simplest quantity with which to do the matching is the neutral pion mass, and this was used to determine the value of ℓ_7 in Ref. [12]. The LO SU(3) result [given in Eq. (3) above] expands to

$$m^2_{\pi^0{\rm SU(3)\,LO}} = \chi_\ell - \frac{\epsilon^2}{4B_0 m_s} + \mathcal{O}\left(\frac{\epsilon^2 m_{u,d}}{B_0 m_s^2}\right). \tag{8}$$

The SU(2) result at NLO is

$$m^2_{\pi^0{\rm SU(2)\,NLO}} = \chi_\ell - \frac{2\ell_7\epsilon^2}{f^2} + \mathcal{O}\left(\frac{\chi_\ell^2}{\Lambda_\chi^2}\right), \tag{9}$$

where $\Lambda_\chi = 4\pi f$ is the chiral scale. The χ_ℓ^2 contributions arise from terms in the NLO chiral Lagrangian (including ℓ_3) as well as from chiral logarithms. Equating these two results one finds [12]

$$\ell_7 = \frac{f^2}{8B_0 m_s}. \tag{10}$$

One can show that with this value for ℓ_7, contributions to all pion n-point amplitudes proportional to ϵ^2/m_s agree in the two theories.

We stress that in this matching we are not taking into account "standard" NLO contributions, i.e. those suppressed relative to LO results by factors of $m_{u,d}/\Lambda_{\rm QCD} \sim (m_\pi/\Lambda_\chi)^2$ (up to logarithms). Such contributions arise in both SU(3) and SU(2) χPT and must be included in a full NLO matching. This is not necessary for our purposes since such terms lead to small isospin-conserving corrections to the vacuum structure and pion masses—they do not introduce qualitatively new effects. By contrast, the ϵ^2 terms that we keep lead to isospin breaking, and are the leading-order contributions which do so. Indeed, for this reason ℓ_7 is not renormalized at this order, since, as already noted, one-loop chiral logarithms do not contain a term

[3]The theory along the $m_u = -m_d$ diagonal is identical to that with $m_u = m_d$ at $\theta_{\rm QCD} = \pi$, and has been discussed extensively in the literature. In particular, a χPT analysis of this theory has been given in Ref. [10].

proportional to ϵ^2. Thus it is consistent to work with the classical potential, rather than the one-loop effective potential. This is not the case for other LECs such as ℓ_3, which are renormalized and thus scale dependent [12].

We can formalize this by noting that standard NLO contributions are parametrically smaller than the terms we keep by a factor of $m_s/\Lambda_{\rm QCD}$. This allows the development of a consistent power-counting scheme in which the ϵ^2 terms are larger than generic m^2 contributions.[4] We discuss this in the following section. To be consistent we should also account for NLO contributions in SU(3) χPT of size $m_s/\Lambda_{\rm QCD}$ relative to LO terms. These, however, lead only to a renormalization of the SU(2) constants f and B_0 relative to their SU(3) counterparts. Since we work henceforth entirely in the SU(2) theory, we choose to leave this renormalization implicit.

We now show that the inclusion of the ℓ_7 term leads to the same phase diagram as found in the LO SU(3) analysis. Given the matching result Eq. (10), we always assume $\ell_7 > 0$ in the following. Using $\langle\Sigma\rangle = \exp(i\theta\hat{n}\cdot\vec{\tau})$, the potential becomes

$$\mathcal{V}_{\rm SU(2)} = -f^2(\chi_\ell \cos\theta + c_\ell \epsilon^2 n_3^2 \sin^2\theta), \qquad (11)$$

where $c_\ell = \ell_7/f^2$. Since $\ell_7 > 0$, the potential is always minimized by choosing $|n_3| = 1$. Since $n_3 = 1$ and $n_3 = -1$ are related by changing the sign of θ, we can, without loss of generality, set $n_3 = 1$. The resulting potential is stationary with respect to θ at the "normal" values $\theta = 0$ and π, and in addition at

$$\cos\theta = \frac{\chi_\ell}{2c_\ell\epsilon^2}. \qquad (12)$$

This new stationary value always leads to the global minimum of the potential where it is valid, i.e. when $|\cos\theta| \le 1$. Thus, for fixed ϵ, there is a new phase for $-2c_\ell\epsilon^2 \le \chi_\ell \le 2c_\ell\epsilon^2$, within which $\langle\Sigma\rangle$ is complex and CP is violated. Although $\cos\theta$ is fixed, the sign of θ is not, with the two possible vacua being related by a CP transformation. This phase matches continuously onto the normal phases with $\cos\theta = \pm 1$ at its boundaries. Thus the phase transition is of second order.

The resulting phase diagram is sketched in Fig. 3. This is not only qualitatively similar to the central portion of the LO SU(3) phase diagram (Fig. 2), but is in fact in complete quantitative agreement at the appropriate order. For example, expanding the SU(3) result for the phase boundary,

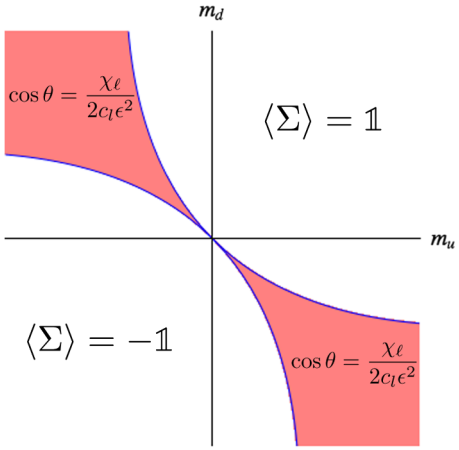

FIG. 3 (color online). Phase diagram from SU(2) χPT including the ℓ_7 term with $\ell_7 > 0$. Equations for the positions of phase transition lines are given in the text.

$m_u = -m_d/(1 + m_d/m_s)$, in powers of $m_{u,d}/m_s$, and keeping only the leading nontrivial term, one finds that the boundary occurs at $\chi_\ell = \epsilon^2/(4B_0 m_s)$. This agrees with the SU(2) result $\chi_\ell = 2\ell_7\epsilon^2/f^2$ using the matching condition (10). We have also checked that the pion masses agree throughout the phase plane. We do not quote results for pion masses here, since they are included in the more general analysis presented below.

The fact that the CP-violating phase can be reproduced within SU(2) χPT was first explained by Smilga [10]. His work considered only the case $m_u = -m_d$, which, as noted above, is the same as $m_u = m_d$ with $\theta_{\rm QCD} = \pi$. The analysis presented here gives the (very simple) generalization to arbitrary nondegenerate quark masses. There is also a close relation between our analysis and the recent work of Aoki and Creutz [11]. These authors do not use χPT *per se*, but rather an effective theory containing both pions and the η meson. If the η were integrated out then their theory would reduce to that we consider here, including the ℓ_7 term, plus small corrections. We think, however, that it is preferable to work in a strict effective theory framework, in which only the light particles are kept as dynamical degrees of freedom.

IV. INCLUDING DISCRETIZATION EFFECTS FOR WILSON-LIKE FERMIONS

In this section we recall how lattice artifacts can be incorporated into χPT, and study their impact on the phase structure described above at leading nontrivial order. We do this for untwisted Wilson-like fermions—twist will be considered in the following sections. The method leads to the chiral effective theory describing lattice simulations close to the continuum limit. We begin by recalling the analysis for degenerate quarks and then add in nondegeneracy. We work entirely in the two-flavor theory obtained after the strange quark (and the charm quark too, if present)

[4]The numerical basis for this power counting is not very strong. For example, ℓ_7 and $\ell_3(\mu)$ are comparable in size for reasonable values of the scale μ. Thus the numerical size of the standard NLO corrections we are dropping may be comparable to those proportional to ϵ^2 that we are keeping. The key point, however, is that we are interested in qualitatively new effects, rather than a precise quantitative description.

has been integrated out. For untwisted Wilson-like fermions (unlike for twisted-mass fermions), the analysis could also be carried out within SU(3) χPT, but there is no advantage to doing so as the dominant long-distance dynamics lies in the SU(2) sector.

Both quark masses and discretization effects break chiral symmetry, and it is important to understand the relative size of these effects. Our focus here is on state-of-the-art simulations, which have $m_{u,d}$ close to their physical values ($m_u \approx 2.5$ MeV and $m_d \approx 5$ MeV in the modified minimal-subtraction scheme at $\mu = 2$ GeV), and lattice spacings such that $1/a \approx 3$ GeV. In this case, the relative size of discretization effects is characterized by $a\Lambda_{\rm QCD} \approx 0.1$ (using $\Lambda_{\rm QCD} = 300$ MeV), so that

$$a\Lambda_{\rm QCD}^2 \approx 30 \text{ MeV} \gg m_{u,d} \approx a^2\Lambda_{\rm QCD}^3 \approx 3 \text{ MeV}. \quad (13)$$

The appropriate power counting is thus (in schematic notation) $a^2 \sim m$. This is the Aoki regime, in which the competition between discretization and mass effects leads to an interesting phase structure [5,6].

Discretization effects can be incorporated into χPT following the method of Ref. [6]. For unimproved (or partially improved) Wilson fermions, the dominant discretization effect is proportional to a. In the pion sector, however, this contribution can be absorbed entirely into a common shift in all quark masses [6], and we assume below that this shift has been made. The first nontrivial discretization effect is that proportional to a^2. This changes the LO potential to [6]

$$\mathcal{V}_{a^2} = -\frac{f^2}{4}\mathrm{tr}(\chi^\dagger\Sigma + \Sigma^\dagger\chi) - W'[\mathrm{tr}(\hat{A}^\dagger\Sigma + \Sigma^\dagger\hat{A})]^2. \quad (14)$$

Here we are using the notation of Ref. [13], in which $\hat{A} = 2W_0 a\mathbb{1}$ is a spurion field, with dimensions of mass squared, and is proportional to the identity matrix in flavor space. W_0 and W' are new LECs.

The analysis of the vacuum structure for degenerate quarks was given in Ref. [6]. Since $\mathcal{V}_{a^2}$ is independent of the ϵ, the results are unchanged at LO in the presence of nondegeneracy. To determine the vacuum we must minimize

$$\mathcal{V}_{a^2} = -f^2(\chi_\ell \cos\theta + w'\cos^2\theta), \quad (15)$$

where $w' = 64W'W_0^2a^2/f^2$. For $w' < 0$, the analysis is essentially the same as that for $\mathcal{V}_{\rm SU(2)}$ with $\ell_7 > 0$, as given in the previous section. Stationary points are at $\cos\theta = \pm 1$ and

$$\cos\theta = -\frac{\chi_\ell}{2w'}, \quad (16)$$

with the latter being the global minimum where valid ($|\cos\theta| \le 1$). This leads to the phase diagram shown in Fig. 4, with an Aoki phase [5] separated from the normal phases by second-order transitions at $|\chi_\ell| = -2w'$. Strictly speaking, the name "Aoki phase" has been applied previously only on the diagonal $m_u = m_d$ axis, but in the present approximation it holds also for nondegenerate quarks. Within the Aoki phase the potential is independent of the direction of the condensate, $\hat{n}$, so that there are two massless Goldstone bosons, the charged pions. Parity and flavor are violated within this phase. With the canonical choice of the direction of the condensate, $\hat{n} = \hat{z}$, CP is also violated.

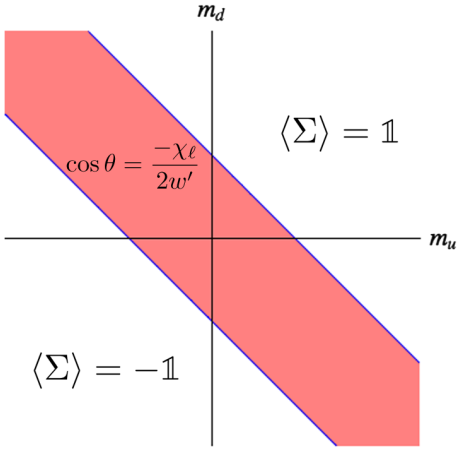

FIG. 4 (color online). Phase diagram in LO SU(2) χPT including discretization effects with $w' < 0$ (Aoki scenario). Equations for the positions of phase transition lines are given in the text.

For $w' > 0$, the global minimum lies at $\cos\theta = \mathrm{sign}(\chi_\ell)$, with a first-order transition at $\chi_\ell = 0$. The phase diagram is thus identical to that in the continuum (Fig. 1). The only difference is that here the yellow line indicates a genuine first-order transition, since on the lattice there are no symmetries connecting the two sides. This case is referred to as the first-order scenario [6].

We are now ready to combine the effects of nondegeneracy with discretization errors. This requires that we adopt an appropriate power-counting scheme for the relative importance of ϵ^2, m and a^2, where m indicates a generic quark mass. Recalling that ϵ^2 terms are enhanced compared to generic m^2 terms we use

$$m \sim a^2 > \epsilon^2 > ma \sim a^3 > a\epsilon^2 > m^2 \sim ma^2 \sim a^4 \ldots. \quad (17)$$

This can be thought of as treating $\epsilon \sim a^{1+\delta}$, with $0 < \delta < 1/2$. The utility of this power counting is that it allows us to first add the ϵ^2 term to those proportional to m and a^2, and then consider terms of order $ma \sim a^3$ at a later stage (in Sec. VII below). Indeed, we could, for the purposes of this section, set $\delta = 0$, and treat the ϵ^2 term as of LO. We do not do so, however, since this would require us to later treat $a\epsilon^2$ terms as of the same size as those proportional to $ma \sim a^3$. Nevertheless, we will loosely describe the inclusion of m, a^2 and ϵ^2 terms as constituting our LO analysis, while treating the $ma \sim a^3$

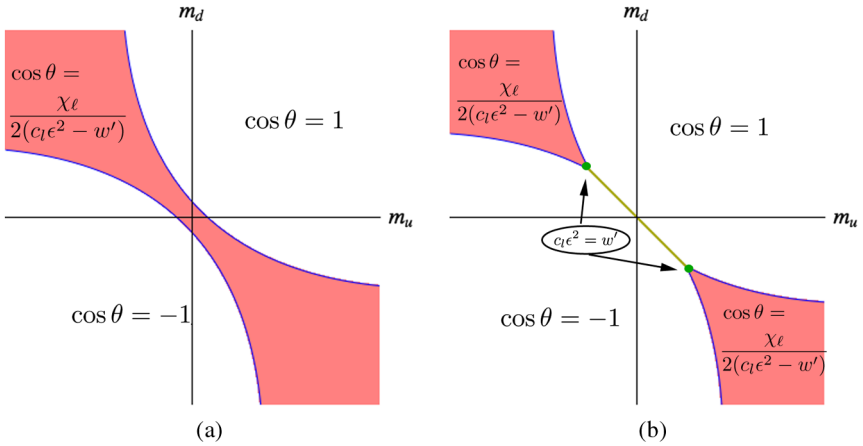

FIG. 5 (color online). Phase diagrams including effects of both discretization and nondegeneracy. Darker (blue) and lighter (yellow) lines indicate transitions of, respectively, second and first order. Equations for the positions of phase transition lines are given in the text. (a) Aoki scenario ($w' \leq 0$). (b) First-order scenario ($w' > 0$).

terms as being of NLO. Terms of yet higher order will not be considered.

With the power counting in hand, we can extend the inclusion of discretization errors into χPT to incorporate the effects of nondegeneracy. This leads to the appearance of new operators in the Symanzik effective Lagrangian, and thus, potentially, to new terms in the chiral Lagrangian. The constraints on additional operators in the Symanzik Lagrangian in the presence of nondegeneracy were worked out in Ref. [14]. Using their results within our power-counting scheme, we find that the lowest-order new operator is $\sim a\epsilon^2\bar{\psi}\psi$. This is, however, of higher order than we consider here.[5] All other operators are of yet higher order. Thus, at the order we work, nondegeneracy only enters our calculation through the continuum ℓ_7 term. The LO potential thus becomes

$$\mathcal{V}_{a^2,\ell_7} = -\frac{f^2}{4}\mathrm{tr}(\chi^\dagger\Sigma + \Sigma^\dagger\chi) - W'[\mathrm{tr}(A^\dagger\Sigma + \Sigma^\dagger A)]^2 + \frac{\ell_7}{16}[\mathrm{tr}(\chi^\dagger\Sigma - \Sigma^\dagger\chi)]^2. \quad (18)$$

We stress that it is self-consistent to determine the vacuum structure and pion masses from a tree-level analysis of $\mathcal{V}_{a^2,\ell_7}$ since loop effects only come in at $\mathcal{O}(m^2, ma^2, a^4)$.

In terms of the parameters of $\langle\Sigma\rangle$, the potential is now given by

$$-\frac{\mathcal{V}_{a^2,\ell_7}}{f^2} = \chi_\ell\cos\theta + c_\ell\epsilon^2 n_3^2\sin^2\theta + w'\cos^2\theta. \quad (19)$$

As before, we can set $n_3 = 1$ without loss of generality. The stationary points are at $\cos\theta = \pm 1$ and

$$\cos\theta = \frac{\chi_\ell}{2(c_\ell\epsilon^2 - w')}. \quad (20)$$

The latter minimizes the potential if $c_\ell\epsilon^2 - w' > 0$ and is valid for $|\cos\theta| \leq 1$. This results in the phase diagrams of Figs. 5(a) and 5(b) for $w' < 0$ and $w' > 0$, respectively. In the former case, corresponding to the Aoki phase for degenerate quarks, the second-order transition lines lie at

$$\chi_\ell = \pm 2(c_\ell\epsilon^2 - w'). \quad (21)$$

Thus the width of the phase grows as $|\epsilon|$ increases. Furthermore, comparing to Fig. 4, we see that the continuum CP-violating phase and the Aoki phase are continuously connected.[6] The only subtlety in this connection is that the condensate definitely points in the n_3 direction for $\epsilon \neq 0$ (i.e. the direction picked out by the nondegenerate part of the mass term), whereas for $\epsilon = 0$ the direction is arbitrary.

In the first-order scenario, Fig. 5(b), the first-order transition along the $m_u = -m_d$ line reaches only to $c_\ell\epsilon^2 = w'$, at which point the CP-violating phase appears. The second-order transition lines are then given by $|\chi_\ell| = 2(c_\ell\epsilon^2 - w')$, i.e. by the same equation as in the Aoki scenario.

We next calculate the pion masses throughout the phase plane, expanding about the vacuum as

$$\Sigma = \exp(i\theta\tau_3)\exp(i\vec{\pi}\cdot\vec{\tau}/f). \quad (22)$$

Outside the CP-violating phase, we find

$$m_{\pi^0}^2 = |\chi_\ell| - 2(c_\ell\epsilon^2 - w'), \quad (23)$$

$$m_{\pi^\pm}^2 = m_{\pi^0}^2 + 2c_\ell\epsilon^2, \quad (24)$$

while within the CP-violating phase we have

[5]Furthermore, when mapped to the chiral Lagrangian, it leads to contributions which can be absorbed by making the untwisted mass m have a weak dependence on ϵ. Thus it does not lead to new phases, but only to a small distortion of the phase diagram.

[6]This result is in agreement with Creutz's conjecture [8].

$$m_{\pi^0}^2 = 2(c_\ell \epsilon^2 - w')\sin^2\theta, \tag{25}$$

$$m_{\pi^\pm}^2 = 2c_\ell \epsilon^2, \tag{26}$$

where θ is given in Eq. (20). These results are plotted vs χ_ℓ for various characteristic choices of ϵ and w' in Fig. 6.

Figures 6(a) and 6(b) show the continuum results for degenerate and nondegenerate masses, respectively. The neutral pion mass vanishes along the second-order transition line, as expected. The full degeneracy at $\chi_\ell = 0$ is due to the fact that the theory regains flavor symmetry (with

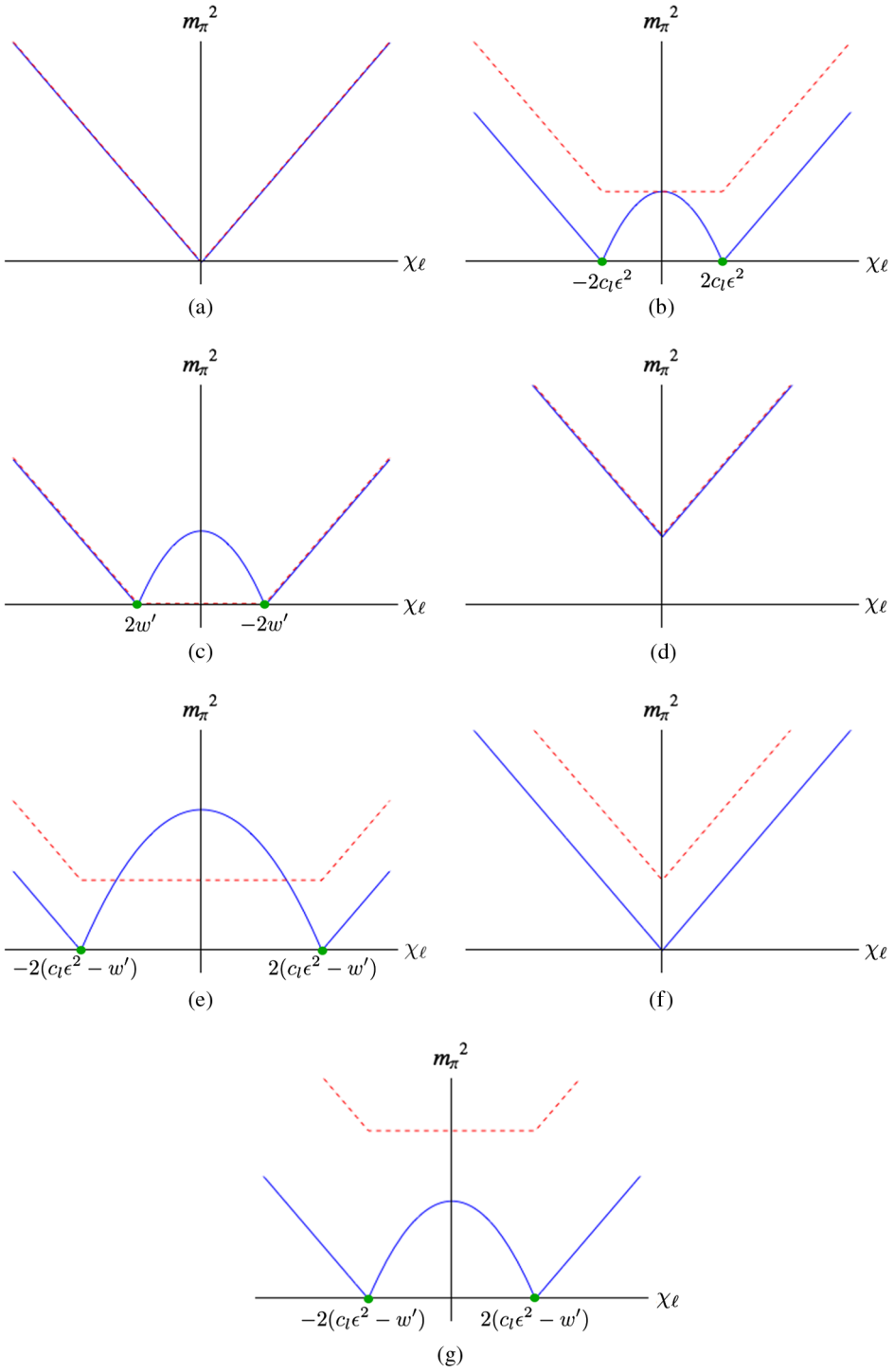

FIG. 6 (color online). Pion masses for untwisted Wilson fermions including the effects of both discretization ($w' \neq 0$) and nondegeneracy ($\epsilon \neq 0$). $m_{\pi^0}^2$ is shown by solid (blue) lines, and $m_{\pi^\pm}^2$ is shown by dashed (red) lines. Explicit expressions for the masses are given in the text. Vertical scales differ between the figures. (a) $w' = c_\ell \epsilon^2 = 0$. (b) $w' = 0$, $c_\ell \epsilon^2 > 0$. (c) $w' < 0$, $c_\ell \epsilon^2 = 0$. (d) $w' > 0$, $c_\ell \epsilon^2 = 0$. (e) $w' < 0$, $c_\ell \epsilon^2 > 0$. (f) $c_\ell \epsilon^2 = w' > 0$. (g) $c_\ell \epsilon^2 > w' > 0$.

$\theta_{\rm QCD} = \pi$) at this point. A characteristic feature of the spectrum at this order is that the charged pion mass is independent of χ_ℓ within the CP-violating phase. This holds also when discretization errors are included.

Figures 6(c) and 6(d) show the spectrum for degenerate quarks with discretization errors included, respectively, for the Aoki and first-order scenarios, reproducing the results of Ref. [6].

Our new results are those of Figs. 6(e)–6(g), which include the effects of both discretization errors and nondegeneracy. In this case the charged and neutral pion masses differ in general. Figure 6(e) shows the behavior in the Aoki scenario, where m_{π^0} vanishes on the phase transition lines, and rises above $m_{\pi^\pm}$ in the central region of the CP-violating phase. There are thus two values of χ_ℓ where all pions are degenerate, but these are accidental degeneracies and not indicative of any symmetry. For the first-order scenario Fig. 6(f) shows the spectrum when ϵ is chosen so that the plot passes through the end point of the second-order transition line, while Fig. 6(g) shows what happens as one moves through the CP-violating phase. In this case, there are no degenerate points.

Simulations using Wilson-like fermions at physical masses, including isospin breaking, have recently begun [7]. What is the significance of our results for such simulations? The main issue is whether discretization effects can move the CP-violating phase such that it lies closer to, or even includes, the physical point. Clearly one wants to avoid simulating in this phase, since it has a different vacuum structure from the continuum theory. But even lying close to a second-order transition could lead to algorithmic issues due to critical slowing down. What we have found is that the phase does move closer to the physical point in the Aoki scenario [Fig. 5(a)]. In this scenario, the CP-violating phase now includes a region of positive quark masses. On the other hand, for the first-order scenario, discretization effects move the CP-violating phase away from the physical point. A positive aspect of our results is that discretization errors lead only to a overall shift in pion masses (outside of the CP-violating phase), so that the difference $m^2_{\pi^\pm} - m^2_{\pi^0}$ takes its continuum value $2c_\ell\epsilon^2$ in both scenarios.

V. TWISTED-MASS FERMIONS AT MAXIMAL TWIST

In this section we extend the previous analysis to twisted-mass fermions [15] at maximal twist. Such fermions have the important practical property of automatic $\mathcal{O}(a)$ improvement [9]. They are being used to simulate QCD with quarks at or near their physical masses [16,17], and isospin breaking is now being included [18]. The main question we address here is the same as for untwisted fermions: how do discretization effects change the continuum phase structure and pion masses?

In the continuum, twisted-mass fermions are obtained by a nonanomalous axial rotation,

$$\begin{aligned}\mathcal{L}_{\rm QCD} &= \bar\psi(D + m_\ell + \epsilon_\ell\tau_3)\psi \\ &\to \bar\psi(D + m_\ell e^{i\gamma_5\tau_1\omega} + \epsilon_\ell\tau_3)\psi \\ &= \bar\psi(D + m + i\gamma_5\tau_1\mu + \epsilon_\ell\tau_3)\psi, \end{aligned} \tag{27}$$

with $m_\ell = (m_u + m_d)/2$, $\epsilon_\ell = (m_u - m_d)/2$, $m = m_\ell\cos\omega$, $\mu = m_\ell \sin\omega$, and ω is the twist angle. Conventionally, m is called the untwisted (average) mass and μ the twisted (average) mass. Choosing the twist in a direction orthogonal to τ_3 leaves the ϵ_ℓ term unchanged. In the continuum this is a convenience, but not a necessity. Once one discretizes D with a Wilson term, however, it is mandatory to twist in a direction orthogonal to τ_3 if one wants to keep the fermion determinant real [19].[7] By convention, this direction is chosen to be τ_1. The rescaled mass matrix that enters χPT is now

$$\begin{aligned}\chi &= \chi_\ell e^{i\tau_1\omega} + \epsilon\tau_3 \\ &= \chi_\ell\cos\omega\mathbb{1} + i\chi_\ell\sin\omega\tau_1 + \epsilon\tau_3 \\ &= \hat m\mathbb{1} + i\hat\mu\tau_1 + \epsilon\tau_3, \end{aligned} \tag{28}$$

and is no longer Hermitian. Here we have defined

$$\hat m = 2B_0 m = \chi_\ell\cos\omega \quad\text{and}\quad \hat\mu = 2B_0\mu = \chi_\ell\sin\omega \tag{29}$$

following Ref. [13].

To determine the effective chiral theory for twisted-mass lattice QCD the first step is to determine the additional operators in the Symanzik Lagrangian that are induced by twisting. As in the untwisted case, the form of the allowed operators can be obtained from the analysis of Ref. [14], which includes both twist and nondegeneracy. In fact, since $\hat\mu^2$ is smaller than ϵ^2 in our power counting, the inclusion of twist does not change the result for the untwisted case, namely that the lowest-order new operator is $\sim a\epsilon^2$ and of higher order than we are working. Thus at LO the extension χPT to include twist and discretization errors is accomplished by simply using the twisted χ of Eq. (28) in the potential $\mathcal{V}_{a^2,\ell_7}$ of Eq. (18).

Using our standard parametrization of $\langle\Sigma\rangle$ this gives

$$-\frac{\mathcal{V}_{a^2,\ell_7}}{f^2} = \hat m\cos\theta + \hat\mu n_1\sin\theta + c_\ell\epsilon^2 n_3^2\sin^2\theta + w'\cos^2\theta. \tag{30}$$

[7] In Ref. [18], which studied twisted-mass nondegenerate fermions, the twist was chosen in the τ_3 direction. This leads to a complex fermion determinant, which is avoided in practice by perturbing at linear order around the isospin-symmetric theory. Because the twist is in the τ_3 direction, our present results do not apply to these simulations. We will discuss the generalization to τ_3 twist (along with the inclusion of electromagnetism) in an upcoming work [20].

We focus in this section on the case of maximal twist, $\hat{m} = 0$, where simple analytic results can be obtained. Even with this simplification, we note that there is competition between terms in three directions in Σ: the twist direction n_1, the nondegeneracy direction n_3, and the identity direction (w' term). Thus we can expect a more complicated phase structure than for untwisted Wilson fermions. Furthermore, since nondegenerate twisted-mass quarks completely break the continuous SU(2) flavor symmetry, we expect, in general, that all three pion masses will differ.

We find the phase diagrams shown in Fig. 7. Note that we are now plotting the average mass along the vertical axis and the difference horizontally. We do this because $\hat{\mu}$ and ϵ are proportional to parameters that enter the twisted-mass lattice action. To compare to the earlier plots, one should rotate those of Fig. 7 by 45° in a clockwise direction. We see that, at maximal twist, it is the Aoki scenario which is preferred, in the sense that the CP-violating phase does not move closer to the physical point. Indeed, the phase diagram in this scenario is identical to that in the continuum (Fig. 3), with the replacement $\chi_\ell \to \hat{\mu}$. In the first-order scenario, by contrast, there is an additional phase [colored green in Fig. 7(b)] which brings lattice artifacts closer to the physical point. Thus the relative merits of the two scenarios are interchanged compared to the untwisted case.

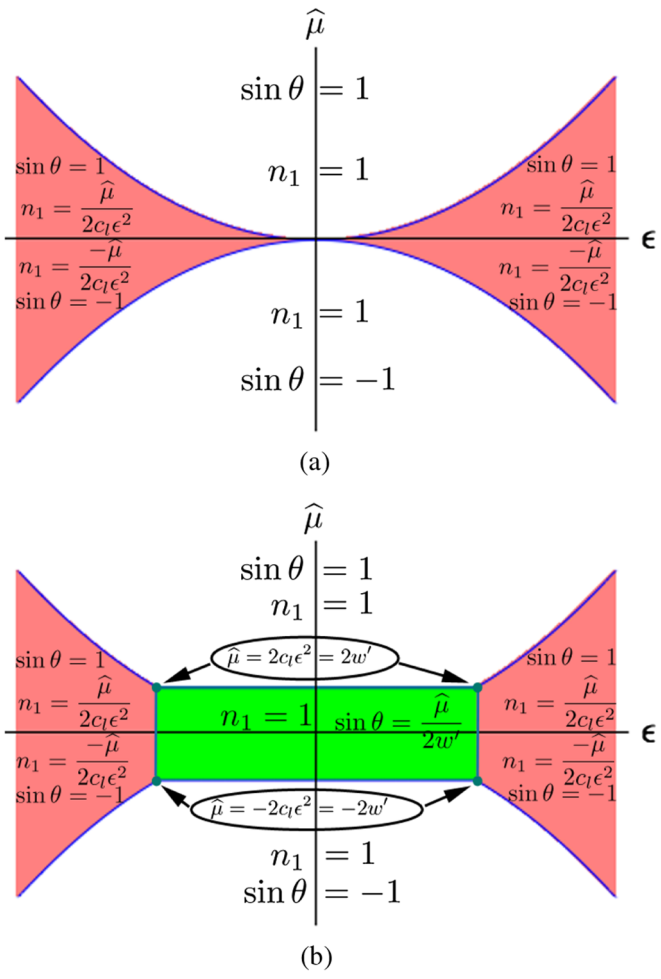

FIG. 7 (color online). Phase diagrams at maximum twist ($\hat{m} = 0$). (a) Aoki scenario or continuum ($w' \leq 0$). (b) First-order scenario ($w' > 0$).

To understand the phase diagrams we first recall the result for the degenerate case, $\epsilon = 0$, which has been studied in Refs. [13,21,22]. These works found, for large $|\hat{\mu}|$, that the condensate is aligned with the twist, i.e. $n_1 = 1$ and $\sin\theta = \text{sign}(\hat{\mu})$. This is as in the continuum. In the Aoki scenario ($w' < 0$), this alignment holds for all $\hat{\mu}$, and there is a first-order transition at $\hat{\mu} = 0$ where $\sin\theta$ changes sign. In the first-order scenario ($w' > 0$), there are second-order transitions at the two points $\hat{\mu} = \pm 2w'$, at which one of the pion masses vanishes. For $|\hat{\mu}| < 2w'$ the condensate smoothly rotates within the group manifold with $\sin\theta = \hat{\mu}/(2w')$. These features are reproduced by our results along the vertical axes in Fig. 7.

We now explain how these results are generalized to $\epsilon \neq 0$. We first observe that we can set $n_2 = 0$. This is because, for any choice of n_1, the c_ℓ term in Eq. (30) (with $c_\ell > 0$) will be minimized when n_3^2 is maximized, i.e. with $n_3^2 = 1 - n_1^2$. Thus there are only two independent variables, θ and n_1. Since n_1 satisfies $|n_1| \leq 1$, we parametrize it as $n_1 = \cos\varphi_1$. Since $\langle\Sigma\rangle$ is invariant when θ and $\hat{n}$ change sign, we need only consider $n_1 \geq 0$, i.e. $0 \leq \varphi_1 \leq \pi/2$. The stationary points are obtained from simultaneously solving

$$\frac{\partial \mathcal{V}_{a^2,\ell_7}}{\partial\theta} \propto \cos\theta[\hat{\mu}\cos\varphi_1 + 2\sin\theta(\sin^2\varphi_1 c_\ell\epsilon^2 - w')] = 0, \tag{31}$$

$$\frac{\partial \mathcal{V}_{a^2,\ell_7}}{\partial\varphi_1} \propto \sin\theta\sin\varphi_1[\hat{\mu} - 2\sin\theta\cos\varphi_1 c_\ell\epsilon^2] = 0. \tag{32}$$

The solutions are as follows:

(1) $\cos\theta = 0$ (so that $\sin\theta = \pm 1$) together with $\sin\varphi_1 = 0$ (so that $n_1 = 1$). In these cases $\mathcal{V}_{a^2,\ell_7}/f^2 = \mp\hat{\mu}$, so that the solution with the lowest energy is that with $\sin\theta = \text{sign}(\hat{\mu})$, giving $\mathcal{V}_{a^2,\ell_7}/f^2 = -|\hat{\mu}|$.

(2) $\sin\theta = \text{sign}(\hat{\mu})$ and $n_1 = \cos\varphi_1 = |\hat{\mu}|/(2c_\ell\epsilon^2)$ so that $\mathcal{V}_{a^2,\ell_7}/f^2 = -\hat{\mu}^2/(4c_\ell\epsilon^2) - c_\ell\epsilon^2$. This is only valid when $n_1 \leq 1$, i.e. $|\hat{\mu}| \leq 2c_\ell\epsilon^2$. There are two degenerate solutions, with $n_3 = \pm\sin\varphi_1$.

(3) $\sin\theta = \hat{\mu}/(2w')$ and $\varphi_1 = 0$ (implying $n_1 = 1$) so that $\mathcal{V}_{a^2,\ell_7}/f^2 = -\hat{\mu}^2/(4w') - w'$. This is only valid when $|\hat{\mu}| \leq 2w'$. There are two degenerate solutions, with opposite signs of $\cos\theta$.

(4) $\cos\theta = \pm 1$ and $\hat{\mu}n_1 = 0$, so that $\mathcal{V}_{a^2,\ell_7}/f^2 = -w'$. This never has lower energy than the third solution and can be ignored.

The first solution is the continuum one discussed above. The second has lower energy than the first where it is valid, and goes over to the CP-violating phase when $w' = 0$.

The third solution is relevant only for $w' > 0$, in which case it has the lowest energy when $c_\ell \epsilon^2 < w'$. The condensate in this phase is independent of ϵ. These considerations lead to the phase diagrams shown in Fig. 7. The potential is continuous throughout the phase planes, as is the condensate except at the junction between the central (green colored) phase and the CP-violating phase in Fig. 7(b). Thus we expect the transitions to be of second order.

We calculate pion masses using the parametrization

$$\Sigma = \exp(i\theta\hat{n}\cdot\vec{\tau}/2)\exp(i\vec{\pi}\cdot\vec{\tau}/f)\exp(i\theta\hat{n}\cdot\vec{\tau}/2), \quad [\langle\Sigma\rangle = \exp(i\theta\hat{n}\cdot\vec{\tau})]. \tag{33}$$

Here we are using an axial transformation to rotate from the twisted basis to the physical basis, which ensures, in the continuum, that the pion fields have physical flavors [23]. In the continuum-like phase (uncolored in the figures), which lies in the regions $|\hat{\mu}| \geq \max(2c_\ell\epsilon^2, 2w')$, we find

$$m_{\pi_1}^2 = |\hat{\mu}| - 2w', \quad m_{\pi_2}^2 = |\hat{\mu}|, \quad m_{\pi_3}^2 = |\hat{\mu}| - 2c_\ell\epsilon^2. \tag{34}$$

These results are consistent with those of Ref. [24], where a χPT calculation in this phase is carried out using the different power-counting $m \gtrsim a$. Various aspects of these results are noteworthy. First, all three masses differ. This is expected since flavor symmetry is completely broken. Second, the charged pions are not mass eigenstates; instead, the eigenstates are $\pi_{1,2}$ and the neutral pion. These two points were also noted in Ref. [24]. Third, one of the pion masses vanishes at each of the phase boundaries: m_{π_3} at the boundary with the CP-violating (pink colored) phase, and m_{π_1} at the boundary with the central (green colored) phase in the first-order scenario.[8] This is expected since these are continuous transitions at which a Z_2 symmetry is broken ($\theta \to -\theta$ for the "green phase" and $n_3 \to -n_3$ for the CP-violating phase). Finally, in the first-order scenario, there are four tricritical points at which *both* m_{π_3} and m_{π_1} vanish. These occur where all three phases meet, i.e. at $|\hat{\mu}| = 2c_\ell\epsilon^2 = 2w'$.

In the central (green) phase we find

$$m_{\tilde{\pi}_1}^2 = 2w' - \frac{\hat{\mu}^2}{2w'}, \quad m_{\pi_2}^2 = 2w', \quad m_{\tilde{\pi}_3}^2 = 2w' - 2c_\ell\epsilon^2. \tag{35}$$

Thus m_{π_2} and m_{π_3} are independent of $\hat{\mu}$ within this phase. These results agree with those in the normal phase [Eq. (34)] at the boundaries. They also show that m_{π_3} vanishes at the borders with the CP-violating (pink) phases ($c_\ell\epsilon^2 = w'$).

In the CP-violating phase there is mixing between π_1 and π_3, with the mass eigenvectors being

$$\tilde{\pi}_1 = n_1\pi_1 + n_3\pi_3 \quad \text{and} \quad \tilde{\pi}_3 = -n_3\pi_1 + n_1\pi_3, \tag{36}$$

where we recall that $n_1 = \hat{\mu}/(2c_\ell\epsilon^2)$ and $n_3 = \sqrt{1-n_1^2}$. The masses are

$$m_{\tilde{\pi}_1}^2 = 2c_\ell\epsilon^2 - 2w', \quad m_{\pi_2}^2 = 2c_\ell\epsilon^2, \quad m_{\tilde{\pi}_3}^2 = 2c_\ell\epsilon^2 - \frac{\hat{\mu}^2}{2c_\ell\epsilon^2}. \tag{37}$$

Note that $m_{\tilde{\pi}_1}$ and m_{π_2} are independent of $\hat{\mu}$, while the $\tilde{\pi}_3$ mass vanishes along the boundaries with the standard phases. The latter result is consistent with the results above because, on these boundaries $|n_1| = 1$ and so $\tilde{\pi}_3 = \pm\pi_3$.

A puzzling feature of these results is what happens at the boundaries between the central (green) and CP-violating (pink) phases. According to Eq. (35) it is the mass of π_3 which vanishes there, while Eq. (37) has the mass of $\tilde{\pi}_1$ vanishing. These appear to be different particles. This is related to a second puzzle, namely that the condensate is discontinuous across the boundary (which lies at $w' = c_\ell\epsilon^2$):

$$\langle\Sigma\rangle_{\text{Green}}^{\text{Boundary}} = i\frac{\hat{\mu}}{2w'}\tau_1 \pm \sqrt{1 - \frac{\hat{\mu}^2}{4w'^2}}\mathbb{1} \quad \text{vs}$$
$$\langle\Sigma\rangle_{\text{Pink}}^{\text{Boundary}} = i\frac{\hat{\mu}}{2w'}\tau_1 \pm i\sqrt{1 - \frac{\hat{\mu}^2}{4w'^2}}\tau_3. \tag{38}$$

Here the $\pm$ signs correspond to the two choices of vacuum state on each side. This situation can be understood by noting that, at the boundary, the vacuum manifold expands to a line which includes all four values of the condensate given in Eq. (38):

$$\langle\Sigma\rangle = i\frac{\hat{\mu}}{2w'}\tau_1 + \sqrt{1 - \frac{\hat{\mu}^2}{4w'^2}}(\cos\phi + i\tau_3\sin\phi), \tag{39}$$

where ϕ is arbitrary. The presence of this flat direction is the reason that one pion is massless, since there is no breaking of a Z_2 symmetry to explain the masslessness. The orientation of the flat direction, which is the direction of the massless pion, depends on the position along this vacuum manifold, and thus is different on the two sides of the transition. In this way the two puzzles above are simultaneously explained.

Results for pion masses are plotted in Fig. 8. We choose the same parameters for the plots as for the untwisted case (Fig. 6) so as to allow a clear comparison. The figures illustrate the discussion given above.

VI. ARBITRARY TWIST

In this section we give a brief discussion of the phase diagram at arbitrary twist. This allows us to understand how the phase diagrams presented above for untwisted and maximally twisted quarks are related to one another. We

[8] In the degenerate case ($\epsilon = 0$) Refs. [13,21,22] found that it is m_{π_3} which vanishes at $|\hat{\mu}| = 2w'$, rather than m_{π_1}. This difference arises because we twist in the τ_1 direction rather than the τ_3 direction used in Refs. [13,21,22].

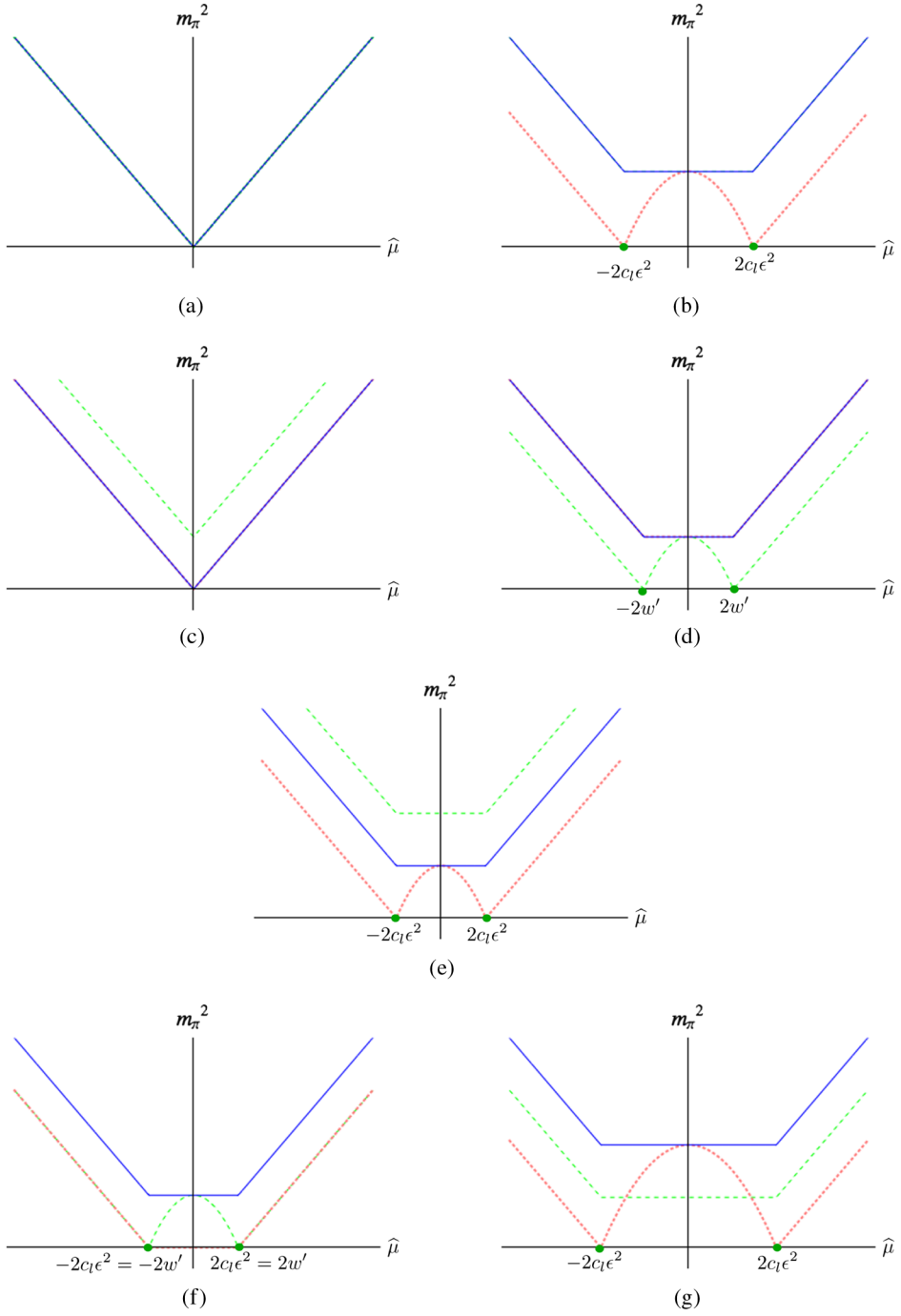

FIG. 8 (color online). Pion masses for maximally twisted fermions including the effects of both discretization ($w' \neq 0$) and nondegeneracy ($\epsilon \neq 0$). $m_{\pi_2}^2$ is shown by solid (blue) lines, $m_{\pi_3}^2$ (and $m_{\tilde{\pi}_3}^2$) by dotted (red) lines and $m_{\pi_1}^2$ (and $m_{\tilde{\pi}_1}^2$) by dashed (green) lines. Not all lines are visible in some figures due to degeneracies. Mixing of pions occurs only within the CP-violating phase in panels (e) and (g). Explicit expressions for masses and mixing are given in the text. Vertical scales differ between the figures. (a) $w' = c_\ell\epsilon^2 = 0$. (b) $w' = 0$, $c_\ell\epsilon^2 > 0$. (c) $w' < 0$, $c_\ell\epsilon^2 = 0$. (d) $w' > 0$, $c_\ell\epsilon^2 = 0$. (e) $w' < 0$, $c_\ell\epsilon^2 > 0$. (f) $w' > 0$, $c_\ell\epsilon^2 = w'$. (g) $w' > 0$, $c_\ell\epsilon^2 > w'$.

focus on the phase diagram, and in particular, the position of the critical manifold where one or more pions are massless.

For arbitrary twist, the potential is given in Eq. (30). As before, minimization leads to $n_2 = 0$, so the potential depends only on θ and φ_1 (defined by $\cos\varphi_1 = n_1$). The equations for stationary points are

$$-\hat{m}\sin\theta + \cos\theta[\hat{\mu}\cos\varphi_1 + 2\sin\theta(c_\ell\epsilon^2\sin^2\varphi_1 - w')] = 0, \tag{40}$$

and Eq. (32). We focus on the case when both $\hat{m}$ and $\hat{\mu}$ are nonzero, since the special cases when one of these vanish have been discussed above.

When $|\hat{\mu}|, |\hat{m}| \gg c_\ell \epsilon^2, |w'|$ the solution which minimizes the potential has

$$n_1 = \cos\varphi_1 = 1, \quad n_3 = \sin\varphi_1, \quad \tan\theta \approx \frac{\hat{\mu}}{\hat{m}}. \tag{41}$$

The last equation becomes an equality in the continuum limit, and simply describes how the condensate twists to compensate the twist in the mass. Discretization errors (here proportional to w') lead to a small deviation in θ from this continuum result. We do not quote the analytic form as it is not illuminating. In fact, the result for θ turns out to be independent of the nondegeneracy ϵ, so the results for the condensate given for the degenerate theory in Refs. [13,21,22] remain valid in this phase. This phase is the extension of the "uncolored" phases in Figs. 5 and 7 to arbitrary twist. At a general position in this phase, the

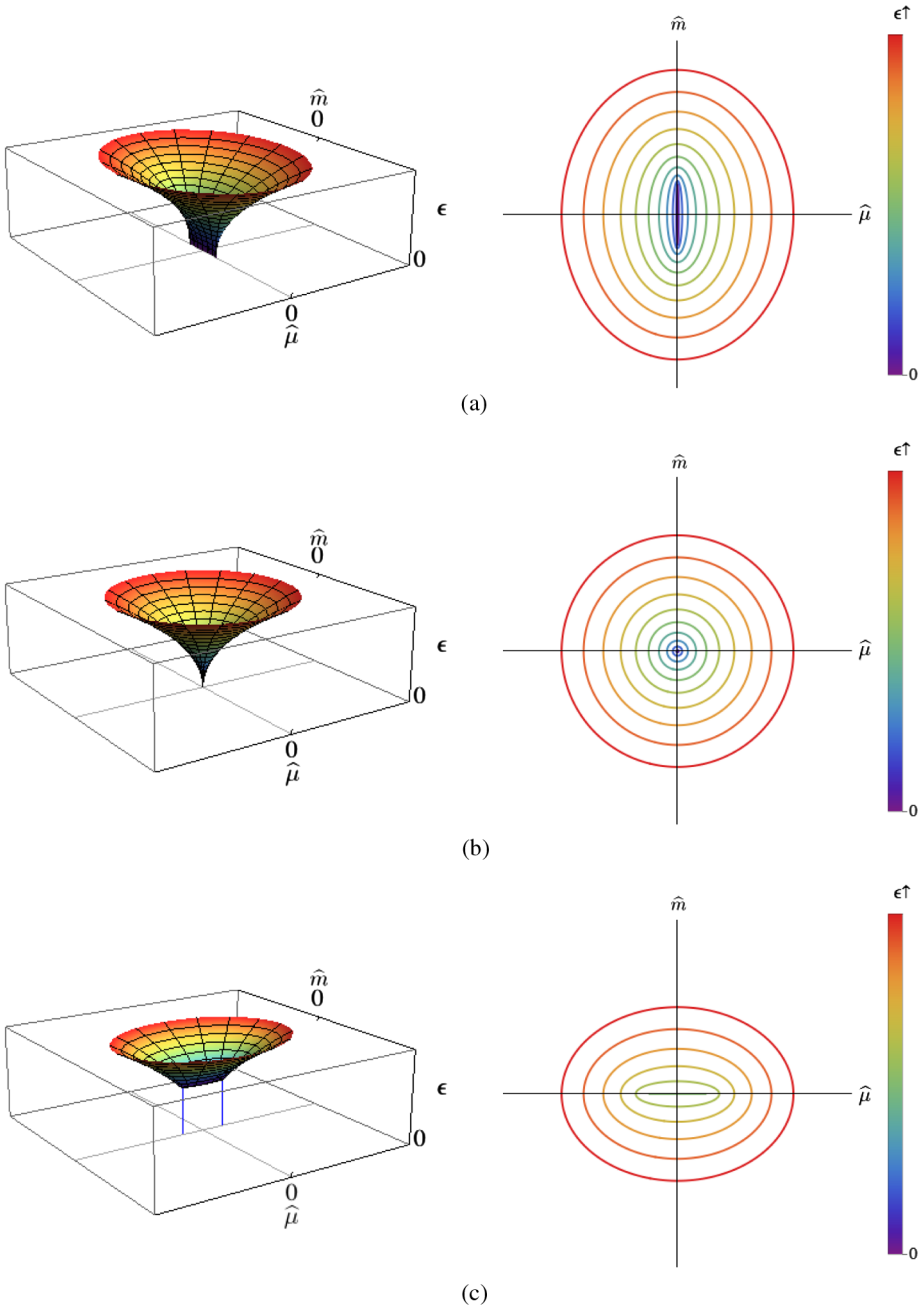

FIG. 9 (color online). Location of the critical manifold for arbitrary twist. Results are shown only for $\epsilon > 0$ since the phase diagrams are symmetric under reflection in the $\epsilon = 0$ plane. The left panels show three-dimensional plots, and the right panels show contour plots. For $w' > 0$, the contour plots do not include the two critical lines which reach down to the $\epsilon = 0$ plane. The scale used for $\hat{m}$ and $\hat{\mu}$ is the same, while that for ϵ is arbitrary. See the text for the equations describing the critical manifold. (a) Aoki scenario ($w' < 0$). (b) Continuum ($w' = 0$). (c) First-order scenario ($w' > 0$).

mass eigenstates are π_1, π_2 and π_3 [using the parametrization of Eq. (33)] and all have different masses.

As ϵ^2 increases, we expect, based on the results of the previous two sections, that we will enter a phase which is connected to the CP-violating (pink) phases found above. This should have a condensate having components in both the n_1 and n_3 directions, and θ taking nonextremal values. Indeed, if $\sin\theta$ and $\sin\varphi_1$ are both nonzero, Eq. (32) is solved by

$$\sin\theta\cos\varphi_1 = \frac{\hat{\mu}}{2c_\ell\epsilon^2}. \tag{42}$$

This requires that $c_\ell\epsilon^2 \geq |\hat{\mu}|$. Inserting this into Eq. (40) then yields

$$\cos\theta = \frac{\hat{m}}{2(c_\ell\epsilon^2 - w')}, \tag{43}$$

which is valid if $2(c_\ell\epsilon^2 - w') \leq \hat{m}$. The solution given by Eqs. (42) and (43) turns out to give the absolute minimum of the potential where it is valid. Its boundary with the continuum-like phase occurs when $|\cos\varphi_1| = 1$, and is thus described by

$$\left(\frac{\hat{m}}{2(c_\ell\epsilon^2 - w')}\right)^2 + \left(\frac{\hat{\mu}}{2c_\ell\epsilon^2}\right)^2 = 1. \tag{44}$$

For fixed ϵ, this is an ellipse in the $\hat{m}$, $\hat{\mu}$ plane. One pion (π_3) is massless along this critical surface.

Within the CP-violating phase all pions are massive, with the mass eigenstates being π_2 and a mixture of π_1 and π_3. The general expressions for these masses are uninformative, and we quote only the results along the boundary of this phase. Here, in addition to the massless π_3 we find

$$m_{\pi_1}^2 = 2c_\ell\epsilon^2 - \frac{2w'\hat{\mu}^2}{(2c_\ell\epsilon^2)^2}, \qquad m_{\pi_2}^2 = 2c_\ell\epsilon^2. \tag{45}$$

The only other critical lines are those we found at maximal twist, namely at $\hat{m} = 0$, $\hat{\mu} = 2w'$ and $c_\ell\epsilon^2 \leq w'$.

The position of the critical manifold resulting from these considerations is shown in Fig. 9 for both scenarios and in the continuum. The CP-violating phases lie within the (distorted) cone-shaped regions. The contour plots show how the circular contours of the continuum are distorted by discretization effects into ellipses. We note that, in the first-order scenario shown in Fig. 9(c), if one passes through any point in the rectangular region in the $(\hat{m}, \epsilon)$ plane between the two critical lines there is a first-order transition at which the condensate changes discontinuously.

VII. HIGHER ORDER

In this section we consider the effect on the previous results of the inclusion of the next highest-order terms in our power counting, i.e. those scaling as $a^3 \sim ma$. At this order we can still determine the vacuum using the classical potential of the chiral theory. The $\mathcal{O}(ma)$ term in this potential is standard; see, e.g. Ref. [25]. The $\mathcal{O}(a^3)$ terms have been discussed for $\epsilon = 0$ in Ref. [26]; the results carry over unchanged to $\epsilon \neq 0$ since the first additional term involving ϵ scales as $a\epsilon^2$ and is of higher order in our power counting. The relevant additional terms entering the potential are

$$\mathcal{V}_{a^3} = -\frac{wf^2}{32W_0 a}\mathrm{tr}(\chi^\dagger\Sigma + \Sigma^\dagger\chi)\mathrm{tr}(A^\dagger\Sigma + \Sigma^\dagger A) - \frac{w_3 f^2}{(8W_0 a)^3}[\mathrm{tr}(A^\dagger\Sigma + \Sigma^\dagger A)]^3, \tag{46}$$

where w and w_3 are new LECs. There is also a term proportional to $\mathrm{tr}(A^\dagger A)\mathrm{tr}(A^\dagger\Sigma + \Sigma^\dagger A)$, but this can removed by (yet another) redefinition of χ. Inserting our standard parametrization $\langle\Sigma\rangle = \exp(i\theta\hat{n}\cdot\vec{\tau})$, and combining the results with that from the LO potential, we obtain

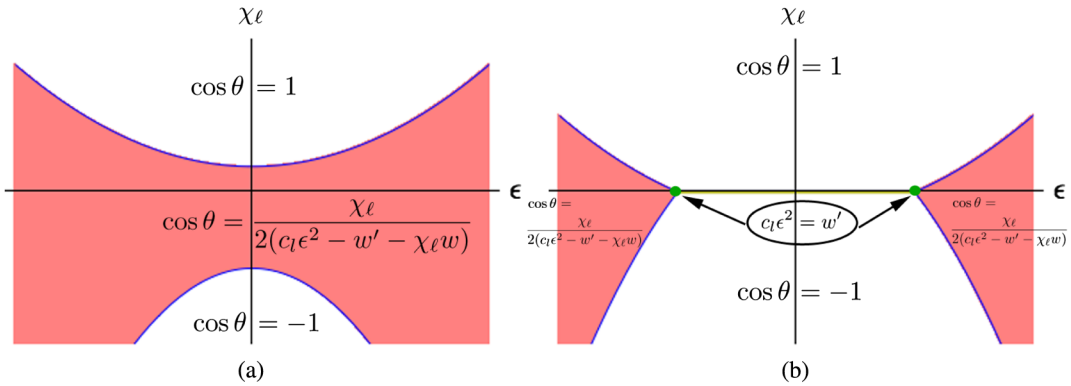

FIG. 10 (color online). Phase diagrams for untwisted Wilson quarks including the NLO $\mathcal{O}(ma)$ term proportional to w. Compare to LO results in Fig. 5. (a) Aoki scenario ($w' < 0$). (b) First-Order Scenario ($w' > 0$).

$$-\frac{\mathcal{V}_{a^2,\ell_7,a^3}}{f^2} = (\hat{m}\cos\theta + \hat{\mu} n_1 \sin\theta)(1 + w\cos\theta) + c_\ell \epsilon^2 n_3^2 \sin^2\theta + w'\cos^2\theta + w_3\cos^3\theta. \quad (47)$$

The new LECs should satisfy $|w| \ll 1$ and $|w_3| \ll |w'|, |c_\ell \epsilon^2|$ in order to be consistent with our power counting.

We begin by considering the untwisted theory, $\hat{\mu} = 0$, where the phase diagram and pion masses can be determined analytically. In this case $\hat{m} = \chi_\ell$. As previously, the potential is minimized with $n_3 = 1$, so that

$$-\frac{\mathcal{V}_{a^2,\ell_7,a^3}}{f^2} \to \chi_\ell \cos\theta(1 + w\cos\theta) + c_\ell \epsilon^2 \sin^2\theta + w'\cos^2\theta + w_3\cos^3\theta. \quad (48)$$

The stationary points satisfy

$$\sin\theta[\chi_\ell - 2(\chi_\ell w - c_\ell \epsilon^2 + w')\cos\theta + 3w_3\cos^2\theta] = 0, \quad (49)$$

which is solved by $\sin\theta = 0$ (i.e. giving the usual continuum solutions with $\cos\theta = \pm 1$) and by the solutions to

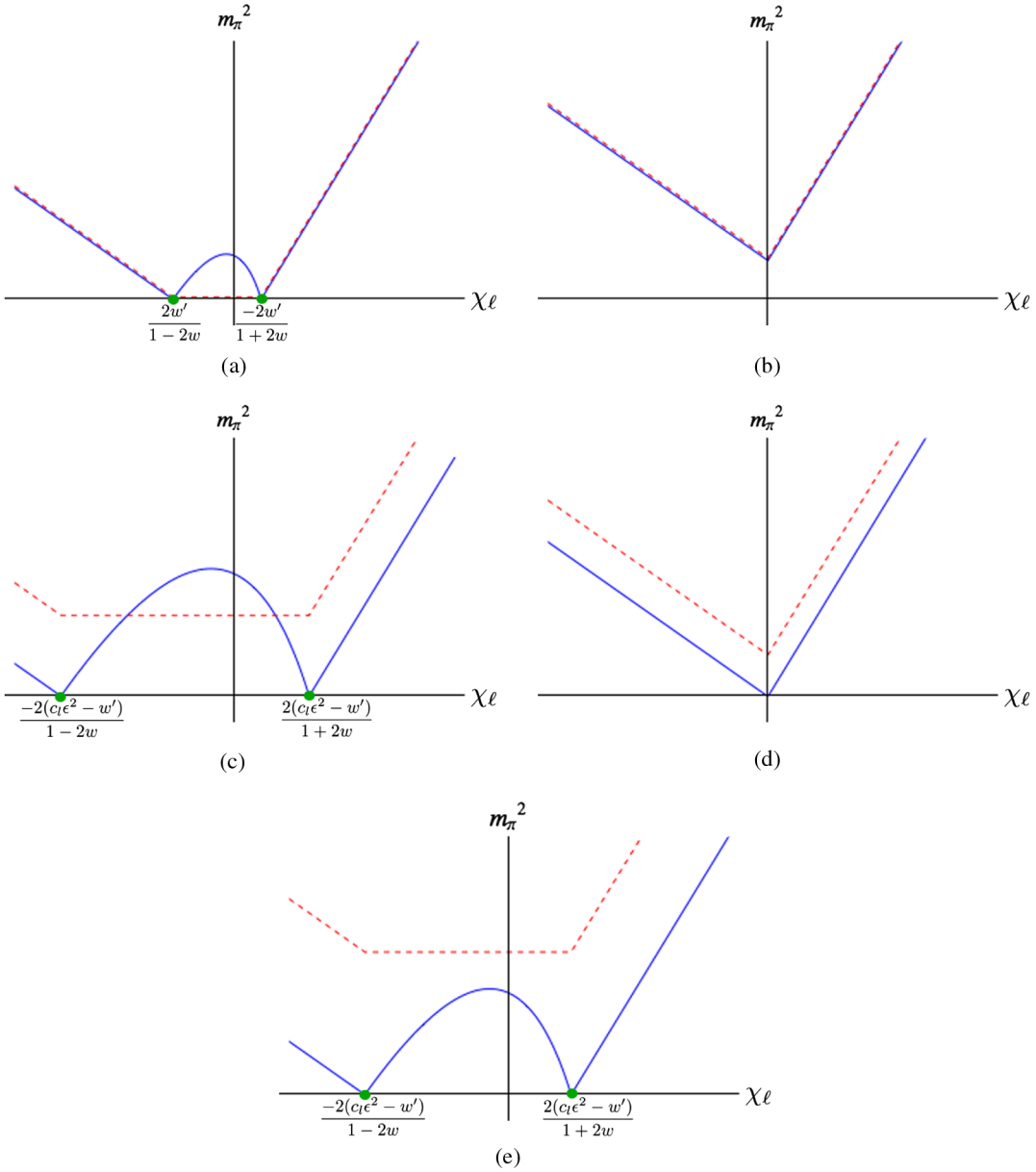

FIG. 11 (color online). Pion masses for untwisted Wilson fermions including the effects of the NLO w term with $w > 0$ (but with $w_3 = 0$). The figures should be compared to the LO results in Figs. 6(c)–6(g), respectively. See Fig. 6 for notation. (a) $w' < 0$, $c_\ell \epsilon^2 = 0$, $w > 0$. (b) $w' > 0$, $c_\ell \epsilon^2 = 0$, $w > 0$. (c) $w' < 0$, $c_\ell \epsilon^2 > 0$, $w > 0$. (d) $c_\ell \epsilon^2 = w' > 0$, $w > 0$. (e) $c_\ell \epsilon^2 > w' > 0$, $w > 0$.

the quadratic function of $\cos\theta$ in parentheses. The latter will lead to CP-violating vacua.

To simplify the discussion we consider the impact of the new terms separately. We first set $w_3 = 0$. Then we can take $w > 0$ without loss of generality, since simultaneously changing $w \to -w$, $\theta \to \theta + \pi$ and $\chi_\ell \to -\chi_\ell$ leaves the potential unaffected. As the w contribution to Eq. (49) leaves the function in parentheses linear in $\cos\theta$, the analysis is little changed from that at LO (see Sec. IV). We find that the CP-violating solution,

$$\cos\theta = \frac{\chi_\ell}{2(c_\ell\epsilon^2 - w' - \chi_\ell w)}, \tag{50}$$

minimizes the potential where it is valid, i.e. wherever $|\cos\theta| < 1$. The endpoints of this phase give second-order transitions occurring at masses

$$\chi_\ell = \pm\frac{2(c_\ell\epsilon^2 - w')}{1 \pm 2w}. \tag{51}$$

Thus the phase boundaries are no longer symmetric with respect to $\chi_\ell = 0$. As in the LO case, if $w' > 0$ and $c_\ell\epsilon^2 < w'$, the transition becomes first order (with the w term having no impact since the transition occurs at $\chi_\ell = 0$). The resultant phase diagrams are shown in Fig. 10.

We have also calculated the pion masses. In the CP-conserving phases the results are

$$m_{\pi^0}^2 = |\chi_\ell|(1 + \mathrm{sign}(\chi_\ell)2w) - 2(c_\ell\epsilon^2 - w'), \tag{52}$$

$$m_{\pi^\pm}^2 = m_{\pi^0}^2 + 2c_\ell\epsilon^2. \tag{53}$$

The only change from the LO results [Eqs. (23) and (24)] is that the slope with respect to χ_ℓ is no longer symmetric when χ_ℓ changes sign. In the CP-violating phases we find

$$m_{\pi^0}^2 = 2(c_\ell\epsilon^2 - w' - \chi_\ell w)\sin^2\theta \quad \text{and} \quad m_{\pi^\pm}^2 = 2c_\ell\epsilon^2, \tag{54}$$

where again only the former result is changed. The resulting pion masses are shown in Fig. 11, and show clearly the above-mentioned asymmetry.

We now consider the impact of the w_3 term, setting $w = 0$. Again, without loss of generality, we can assume $w_3 > 0$. The CP-violating stationary points are now obtained from Eq. (49) by solving a quadratic equation, leading to the solutions

$$\cos\theta_\pm = \frac{(c_\ell\epsilon^2 - w') \pm \sqrt{(c_\ell\epsilon^2 - w')^2 - 3\chi_\ell w_3}}{3w_3}. \tag{55}$$

It is straightforward to see from the properties of a cubic that, since $w_3 > 0$, only the θ_- solution can lead to a minimum of the potential. Whether it does lead to a minimum is a more subtle question than in the LO analysis.

We begin by discussing the limit of small $|w_3|$. Specifically, if we assume $|c_\ell\epsilon^2 - w'| \sim |\chi_\ell| \gg |w_3|$, the

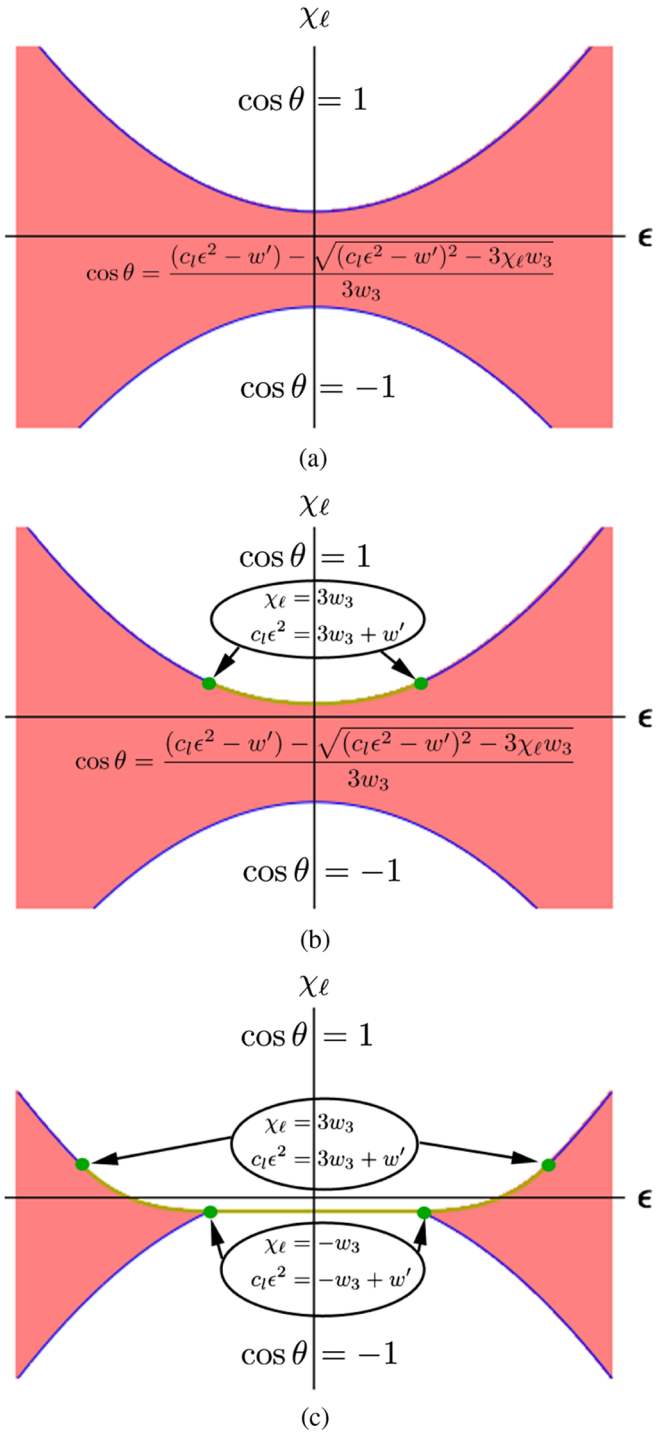

FIG. 12 (color online). Phase diagrams for untwisted Wilson fermions including the NLO $\mathcal{O}(a^3)$ term proportional to w_3. Compare to LO results in Fig. 5. (a) Aoki scenario with $w' < -3w_3 < 0$. (b) Aoki or first-order scenario with $-3w_3 < w' < w_3$ (and $w_3 > 0$). (c) First-order scenario with $w' > w_3 > 0$; $\cos\theta$ in pink region is as is in (a) and (b).

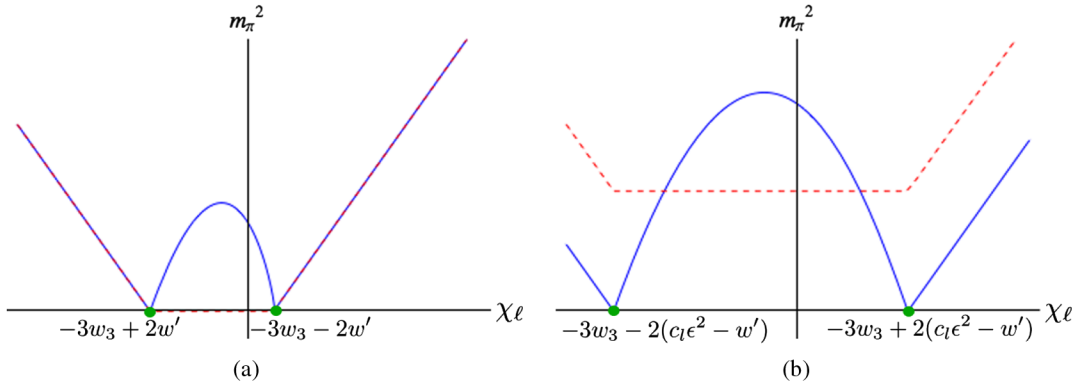

FIG. 13 (color online). NLO pion masses for untwisted Wilson fermions with $w_3 > 0$ and $w = 0$. Results are for the Aoki scenario with $w' < -3w_3 < 0$, corresponding to the phase diagram of Fig. 12(a). Notation is as in Fig. 6. (a) $c_\ell\epsilon^2 = 0$, $-w' < -3w_3 < 0$. (b) $c_\ell\epsilon^2 > 0$, $-w' < -3w_3 < 0$.

square root in Eq. (55) can be expanded in powers of w_3. It is then straightforward to show that one recovers the LO results aside from small corrections proportional to $|w_3/(c_\ell\epsilon^2 - w')|$. In particular, if $c_\ell\epsilon^2 - w' > 0$ there is a CP-violating phase ending in second-order transitions to continuum-like phases, while if $c_\ell\epsilon^2 - w' < 0$ there is a first-order transition.

The positions of these transitions are, however, shifted slightly by the w_3 term. The boundaries of the CP-violating phase occur when $\cos\theta_- = \pm 1$ which gives

$$\chi_\ell = \pm 2(c_\ell\epsilon^2 - w') - 3w_3, \tag{56}$$

without any $\mathcal{O}(w_3^2)$ corrections. In words, the boundaries are simply offset from the LO result [Eq. (21)] by $-3w_3$. In the first-order scenario, the transition occurs at the value of χ_ℓ such that the potentials at $\cos\theta = \pm 1$ agree. This happens when

$$\chi_\ell = -w_3, \tag{57}$$

so that the first-order transition line is offset from the LO result $\chi_\ell = 0$ by $-w_3$ (again, without any higher-order corrections).

More interesting changes occur when $|c_\ell\epsilon^2 - w'| \sim |w_3|$. Note that this does not require that w_3 be large, but rather that there is a cancellation between the $c_\ell\epsilon^2$ and w' terms. Here we encounter a phenomenon first noted at $\epsilon = 0$ in Ref. [26]: one can have a *first-order* transition from the continuum-like phase into the CP-violating phase, followed by a second-order transition to the other continuum-like phase. This occurs when the local minimum at θ_- (with $|\cos\theta_-| < 1$ and $\cos\theta_-$ real) has the same potential as that at $\cos\theta = 1$. Then, as χ_ℓ is reduced, θ jumps from $\theta = 0$ to θ_-. This is possible with a cubic potential, but not with a quadratic. Solving

$$\mathcal{V}_{a^2,\ell_7,a^3}(\theta_-) = \mathcal{V}_{a^2,\ell_7,a^3}(0) \tag{58}$$

leads to the following equation for the first-order boundary:

$$\chi_\ell = \frac{(w' - c_\ell\epsilon^2 - 3w_3)(w' - c_\ell\epsilon^2 + w_3)}{4w_3}. \tag{59}$$

As one moves along this boundary $\cos\theta_-$ varies. The boundary ends when either $\cos\theta_- = 1$, so there is no jump in θ, and the transition becomes second order, or when $\cos\theta_- = -1$, so there is only a first-order transition without the subsequent CP-violating phase. Combining Eqs. (55) and (59) we find that the transition becomes second order at

$$\chi_\ell = c_\ell\epsilon^2 - w' = 3w_3, \tag{60}$$

while it becomes first order at

$$\chi_\ell = c_\ell\epsilon^2 - w' = -w_3. \tag{61}$$

The first of these equations can be satisfied if $w' > -3w_3$, and so reaches from the first-order scenario ($w' > 0$) into a small region of the Aoki scenario. The second requires $w' > w_3$ and thus occurs only in the first-order scenario.

These results lead to the phase diagrams shown in Fig. 12. We see that the changes due to the w_3 term are more substantive than those due to the w term.

We show the corresponding pion masses in Figs. 13–15; for the sake of brevity we do not quote the analytic forms. Figure 13 shows two "slices" through the phase diagram of Fig. 12(a). These should be compared to the LO results in Figs. 5(c) and 5(e), respectively.

In Fig. 14 we show two slices through the phase diagram of Fig. 12(b). The first, at $\epsilon = 0$, shows the first-order transition, at which all pion masses are discontinuous. The charged pions become massless in the CP-violating/Aoki phase, while the neutral pion is massive. In the second slice, for which ϵ satisfies $0 < c_\ell\epsilon^2 < w' + 3w_3$, the discontinuities remain, but all pions are massive in the CP-violating phase (except at the lower boundary where the neutral pion mass vanishes). Once $c_\ell\epsilon^2 \geq w' + 3w_3$, the pion masses behave as in Fig. 13(b).

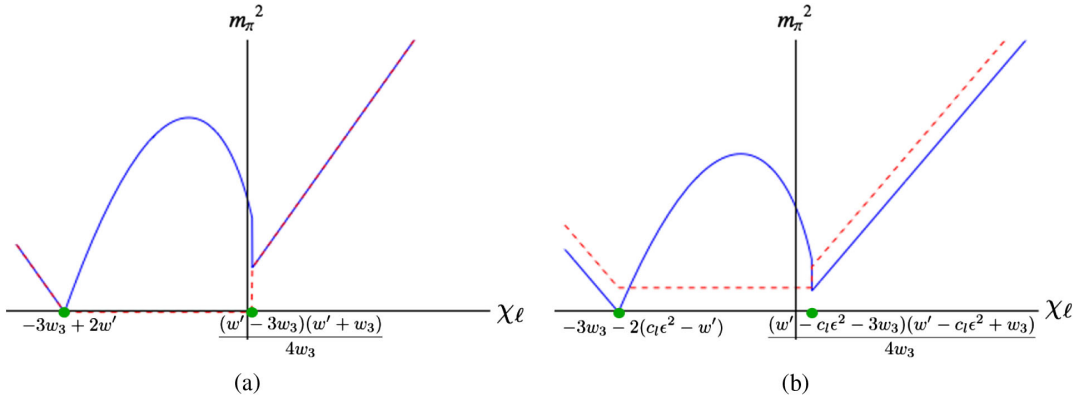

FIG. 14 (color online). Examples of NLO pion masses for untwisted Wilson fermions with $w_3 > 0$ and $w = 0$. Results are for $-3w_3 < w' < w_3$, corresponding to the phase diagram of Fig. 12(b). (a) $c_\ell\epsilon^2 = 0$, $-3w_3 < w' < w_3$. (b) $c_\ell\epsilon^2 \geq w' + 3w_3$, $-3w_3 < w' < w_3$.

In Fig. 15 we show four slices through the phase diagram of Fig. 12(c). The first (at $\epsilon = 0$) shows how the w_3 term leads to a discontinuity in the pion masses at the first-order transition, unlike at LO. This was first observed in Ref. [26]. For nonzero ϵ, the charged and neutral pions are no longer degenerate, and both have a discontinuity. When one reaches $c_\ell\epsilon^2 = w' - w_3$, the neutral pion becomes massless at the transition point, as shown in the second slice. This is the beginning of the CP-violating phase. As ϵ^2 increases further, one has both first- and second-order transitions, as shown in the third slice. The final slice shows the value of ϵ^2 at which the first-order transition turns into a second-order transition. For larger values of ϵ^2 the pion masses behaves as in Fig. 13(b).

The higher-order analysis in the twisted case is more complicated. Maximal twist no longer occurs, in general, at

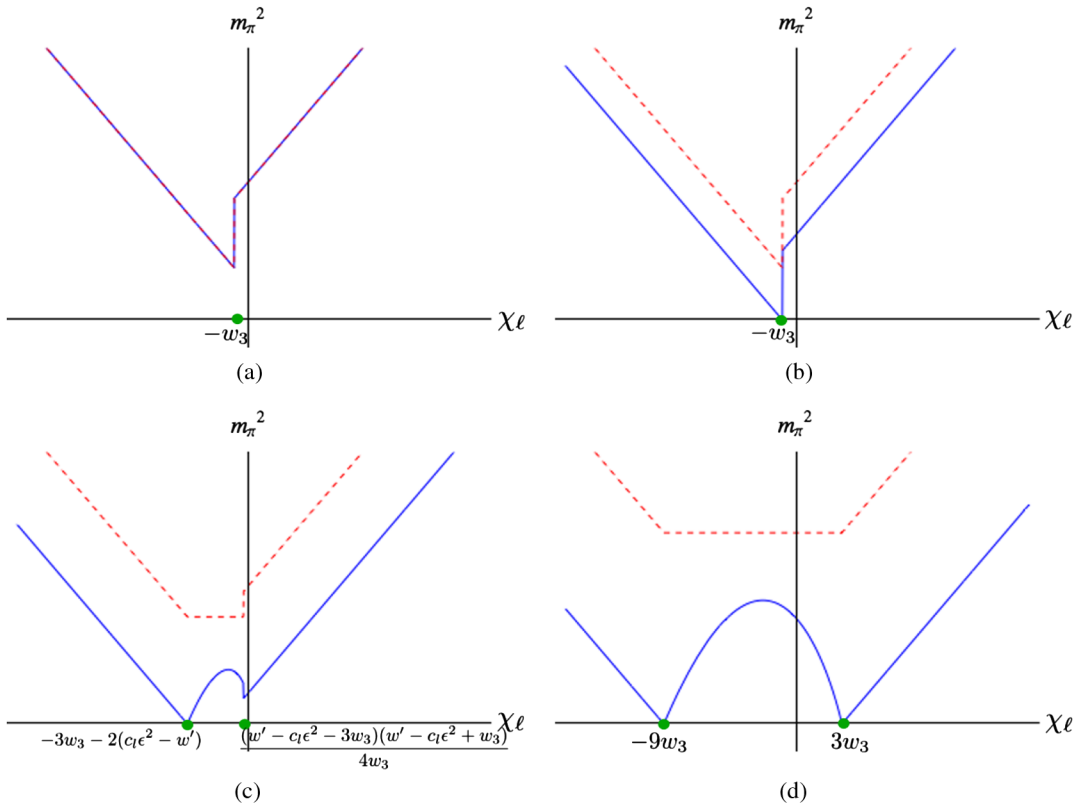

FIG. 15 (color online). NLO pion masses for untwisted Wilson fermions with $w_3 > 0$ and $w = 0$. Results are for the first-order scenario with $w' > w_3$, corresponding to the phase diagram of Fig. 12(c). (a) $c_\ell\epsilon^2 = 0$, $w' > w_3 > 0$. (b) $c_\ell\epsilon^2 = w' - w_3$, $w' > w_3 > 0$. (c) $w' - w_3 < c_\ell\epsilon^2 < w' + 3w_3$, $w' > w_3 > 0$. (d) $c_\ell\epsilon^2 = w' + 3w_3$, $w' > w_3 > 0$.

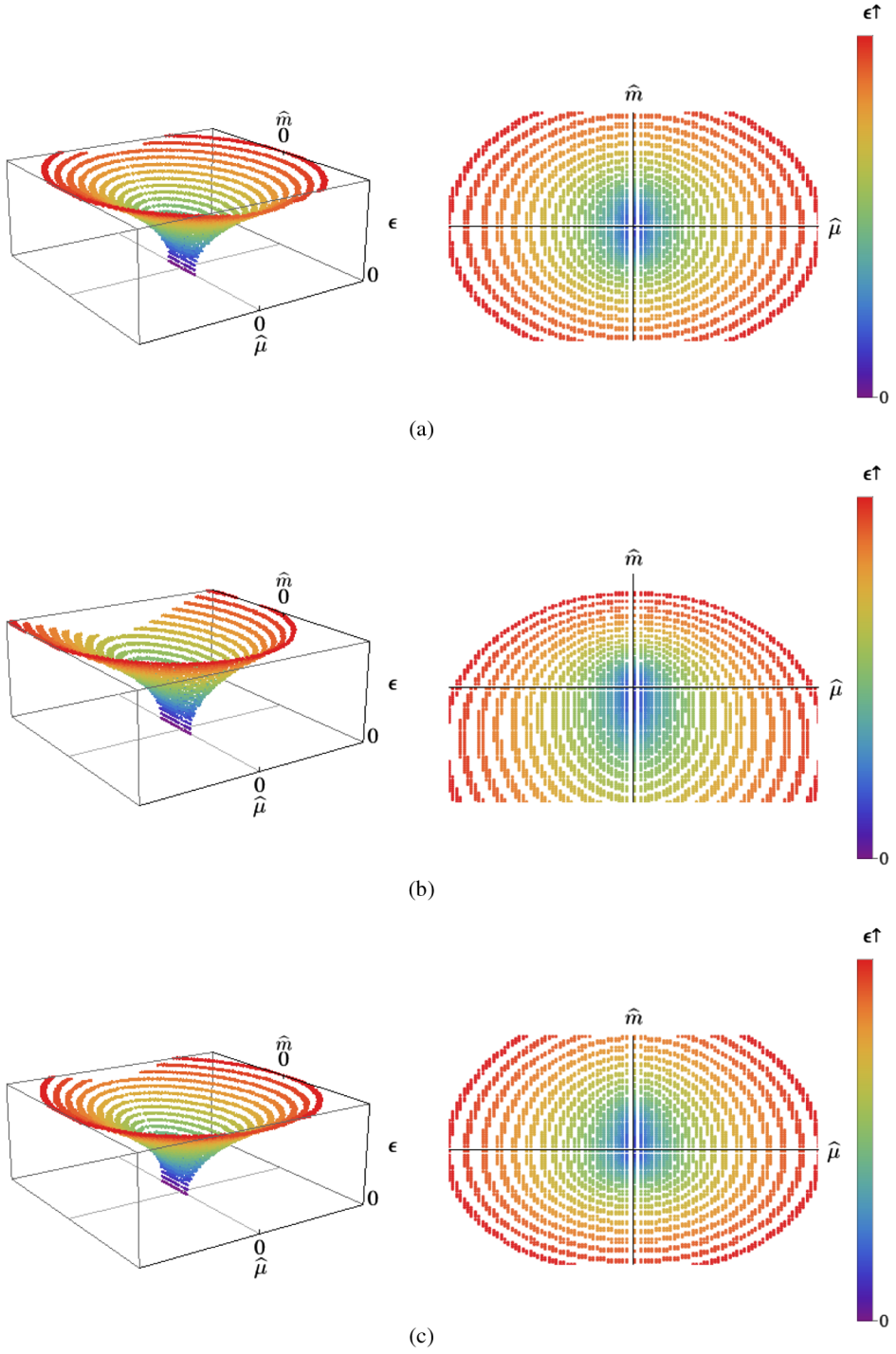

FIG. 16 (color online). Location of the critical manifold in the Aoki scenario ($w' < 0$) including NLO terms. Notation is as in Fig. 9. (a) $w_3 = w = 0$. (b) $w_3 = 0$, $w > 0$. (c) $w' < -3w_3 < 0$, $w = 0$.

$\hat{m} = 0$, so one is forced to do the analysis for both $\hat{m}$ and $\hat{\mu}$ nonvanishing. In practice, this requires numerical minimization of the potential. The resulting phase diagram and pion masses for $\epsilon = 0$ have been discussed in detail in Ref. [26]. The addition of isospin breaking leads both to small quantitative changes, and to qualitative changes in small regions of the phase plane. We restrict ourselves here to showing how the NLO terms impact the critical manifold (on which at least one pion is massless). The Aoki and first-order scenarios are shown, respectively, in Figs. 16 and 17.

The main effect is a distortion of the elliptical cross sections of the critical manifold. In addition, the two vertical critical lines in the first-order scenario are shifted

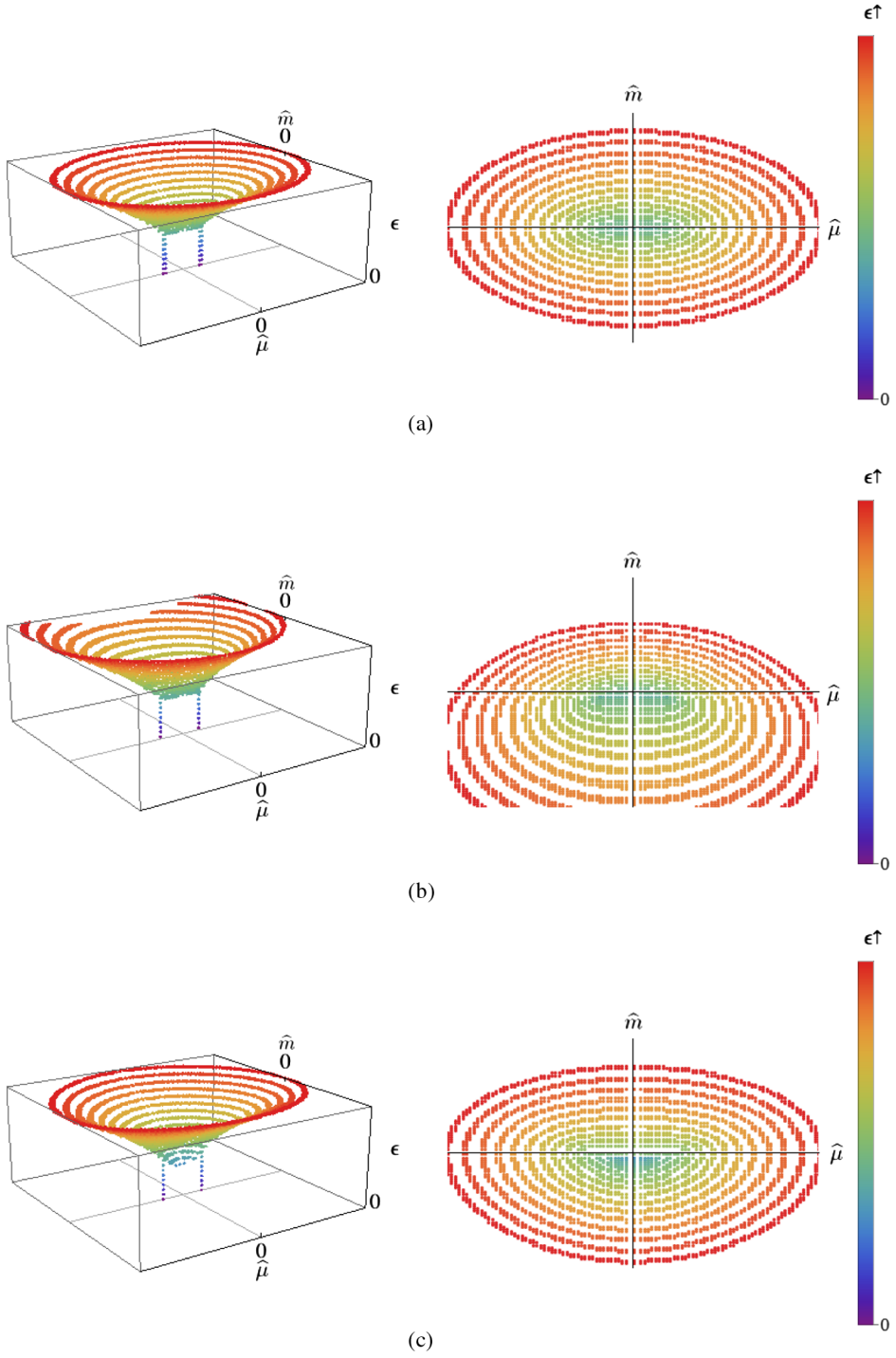

FIG. 17 (color online). Location of the critical manifold in the first-order scenario ($w' > 0$) including NLO terms. Notation is as in Fig. 9. (a) $w_3 = w = 0$. (b) $w_3 = 0$, $w > 0$. (c) $w' > w_3 > 0$, $w = 0$.

slightly in position. The most significant qualitative change is the appearance of a hole in the manifold when $w' > w_3 > 0$, which is (barely) visible above the $\hat{\mu} = 0$ axis in the right panel of Fig. 17(c). This occurs because of the extended first-order transition region seen in the untwisted phase diagram of Fig. 12(c).

We end this section by addressing the question of whether higher-order effects move unphysical phases closer to the point with physical masses. The answer depends on the sign of w and w_3. For untwisted fermions, the results of Figs. 10–17, show that positive w and w_3 move unphysical phases away from the physical point. Conversely, negative values of these LECs would move the phases closer. For twisted-mass fermions the answer is more complicated, depending on the choice of twist angle.

VIII. CONCLUSIONS

In this work we have studied how using nondegenerate up and down quarks changes the phase structure caused by competition between quark mass and discretization effects. We draw two main conclusions. First, the continuum CP-violating phase is continuously connected to the Aoki phase induced by discretization effects. Second, discretization effects can move the theory with physical quark masses closer to, or even into, unphysical phases. Whether this happens depends on both the twist angle and the details of the discretization (the latter impacting the values of the LECs w', etc.). Our overall message is that a complicated phase structure lies in the vicinity of the physical point and simulations should be careful to avoid unphysical phases.

For twisted-mass fermions our results for pion masses extend those of Ref. [24] into the Aoki regime ($m \sim a^2$). In the continuum-like phase, with both twisting and nondegeneracy, the eigenstates are π_1, π_2 and π_3, with all three pions having different masses. Our formulas may be of use in removing the discretization effects from masses determined in simulations, although we stress again that $\mathcal{O}(m^2)$ terms dropped in our power counting may be important if precision fitting is required.

One shortcoming of this work is that it does not include electromagnetic effects. In the pion sector, these lead to isospin breaking that is generically larger than that from quark nondegeneracy, and can also impact the phase structure.[9] We will discuss the impact of electromagnetism in an upcoming work, building upon the recent analysis of Ref. [28].

ACKNOWLEDGMENTS

We thank Mario Kieberg and Jac Verbaarschot for discussions and comments. This work was facilitated through the use of advanced computational, storage, and networking infrastructure provided by the Hyak supercomputer system at the University of Washington. This work was supported in part by the United States Department of Energy Grants No. DE-FG02-96ER40956 and No. DE-SC0011637.

[9] Another generalization that one can consider is the inclusion of an isospin chemical potential. This has been discussed recently for degenerate quarks in Ref. [27].

[1] R. F. Dashen, Phys. Rev. D **3**, 1879 (1971).
[2] M. Creutz, Phys. Rev. Lett. **92**, 201601 (2004).
[3] J. Beringer *et al.* (Particle Data Group), Phys. Rev. D **86**, 010001 (2012).
[4] S. Aoki *et al.*, Eur. Phys. J. C **74**, 2890 (2014).
[5] S. Aoki, Phys. Rev. D **30**, 2653 (1984).
[6] S. R. Sharpe and R. Singleton, Jr., Phys. Rev. D **58**, 074501 (1998).
[7] S. Borsanyi *et al.*, arXiv:1406.4088.
[8] M. Creutz (private communications and seminars).
[9] R. Frezzotti and G. Rossi, J. High Energy Phys. 08 (2004) 007.
[10] A. V. Smilga, Phys. Rev. D **59**, 114021 (1999).
[11] S. Aoki and M. Creutz, Phys. Rev. Lett. **112**, 141603 (2014).
[12] J. Gasser and H. Leutwyler, Nucl. Phys. **B250**, 465 (1985).
[13] S. R. Sharpe and J. M. Wu, Phys. Rev. D **70**, 094029 (2004).
[14] A. Walker-Loud and J. M. Wu, Phys. Rev. D **72**, 014506 (2005).
[15] R. Frezzotti, P. A. Grassi, S. Sint, and P. Weisz (Alpha Collaboration), J. High Energy Phys. 08 (2001) 058.
[16] A. Abdel-Rehim *et al.*, *Proc. Sci.*, LATTICE2013 (2013) 264 [arXiv:1311.4522].
[17] N. Carrasco *et al.* (European Twisted Mass Collaboration), Nucl. Phys. **B887**, 19 (2014).
[18] G. de Divitiis, R. Frezzotti, V. Lubicz, G. Martinelli, R. Petronzio, G. C. Rossi, F. Sanfilippo, S. Simula, and N. Tantalo (RM123 Collaboration), Phys. Rev. D **87**, 114505 (2013).
[19] R. Frezzotti and G. Rossi, Nucl. Phys. B, Proc. Suppl., **128**, 193 (2004).
[20] D. P. Horkel and S. R. Sharpe (to be published).
[21] G. Munster, J. High Energy Phys. 09 (2004) 035.
[22] L. Scorzato, Eur. Phys. J. C **37**, 445 (2004).
[23] S. R. Sharpe and J. M. Wu, Phys. Rev. D **71**, 074501 (2005).
[24] G. Munster and T. Sudmann, J. High Energy Phys. 08 (2006) 085.
[25] G. Rupak and N. Shoresh, Phys. Rev. D **66**, 054503 (2002).
[26] S. R. Sharpe, Phys. Rev. D **72**, 074510 (2005).
[27] M. Kieberg, K. Splittorff, J. Verbaarschot, and S. Zafeiropoulos, in Proceedings of Lattice 2014, Columbia University, New York, 2014 (to be published).
[28] M. Golterman and Y. Shamir, Phys. Rev. D **89**, 054501 (2014).